Title
Current and potential imaging applications of ferumoxytol for magnetic resonance imaging

Authors
Toth, Gerda B
Varallyay, Csanad G
Horvath, Andrea
et al.

Peer reviewed

Current and Potential Imaging Applications of Ferumoxytol for Magnetic Resonance Imaging

Gerda B Toth, MD[1,*], **Csanad G Varallyay, MD, PhD**[2,*], **Andrea Horvath, MD, PhD**[1,*], **Mustafa R Bashir, MD**[3,4], **Peter L Choyke, MD**[5], **Heike E Daldrup-Link, MD, PhD**[6], **Edit Dosa, MD, PhD**[7], **John Paul Finn, MD**[8], **Seymur Gahramanov, MD**[9], **Mukesh Harisinghani, MD**[10], **Iain Macdougall, MD**[11], **Alexander Neuwelt, MD**[12], **Shreyas S Vasanawala, MD, PhD**[13], **Prakash Ambady, MD**[1], **Ramon Barajas, MD**[2], **Justin S Cetas, MD, PhD**[14], **Jeremy Ciporen, MD**[14], **Thomas J DeLoughery, MD**[15], **Nancy D Doolittle, PhD**[1], **Rongwei Fu, PhD**[16,17], **John Grinstead, PhD**[18], **Alexander R Guimaraes, MD, PhD**[2], **Bronwyn E Hamilton, MD**[2], **Xin Li, PhD**[19], **Heather McConnell, BS**[1], **Leslie L Muldoon, PhD**[1], **Gary Nesbit, MD**[2], **Joao P Netto, MD**[1,2], **David Petterson**[2], **William D Rooney, PhD**[19], **Daniel Schwartz, BA**[1,19], **Laszlo Szidonya, MD, PhD**[1], and **Edward A Neuwelt, MD**[1,14,20]

[1]Department of Neurology, Oregon Health & Science University, Portland, Oregon, USA

[2]Department of Radiology, Oregon Health & Science University, Portland, Oregon, USA

[3]Department of Radiology, Duke University Medical Center, 3808, Durham, North Carolina, USA

[4]Center for Advanced Magnetic Resonance Development, Duke University Medical Center, Durham, North Carolina, USA

[5]Molecular Imaging Program, Center for Cancer Research, National Cancer Institute, National Institutes of Health, Bethesda, Maryland 20892-1088, USA

[6]Department of Radiology, Section of Pediatric Radiology, Lucile Packard Children's Hospital, Stanford University, 725 Welch Rd, Stanford, California 94305-5654, USA

[7]Heart and Vascular Center, Semmelweis University, Budapest, Hungary

[8]Department of Radiological Sciences, David Geffen School of Medicine, University of California, Los Angeles, California, USA

[9]Department of Neurosurgery, University of New Mexico Health Sciences Center, Albuquerque, New Mexico, USA

[10]Department of Radiology, Harvard Medical School, Massachusetts General Hospital, Boston, Massachusetts, USA

Corresponding Author: Edward A. Neuwelt, MD, Blood-Brain Barrier Program, Oregon Health & Science University, Portland, OR 97239, neuwelte@ohsu.edu, Phone: 503-494-5626, Fax: 503-494-5627.
*These authors contributed equally to this manuscript.

Authors Conflicts of Interest:

The authors have no conflicts of interest to disclose.

[11]Department of Renal Medicine, King's College Hospital, London, UK

[12]Division of Medical Oncology, University of Colorado Denver, Aurora, Colorado, USA

[13]Department of Radiology, Stanford University, Stanford, California, USA

[14]Department of Neurosurgery, Oregon Health & Science University, Portland, Oregon, USA

[15]Department of Hematology and Medical Oncology, Oregon Health & Science University, Portland, Oregon, USA

[16]School of Public Health, Oregon Health & Science University, Portland, Oregon, USA

[17]Department of Medical Informatics and Clinical Epidemiology, Oregon Health & Science University, Portland, Oregon, USA

[18]Siemens AG, Healthcare Center, Portland, Oregon, USA

[19]Advanced Imaging Research Center, Oregon Health & Science University, Portland, Oregon, USA

[20]Portland Veterans Affairs Medical Center, Portland, Oregon, USA

Abstract

Contrast-enhanced magnetic resonance imaging (MRI) is a commonly used diagnostic tool. Compared to the standard gadolinium-based contrast agents, ferumoxytol (Feraheme, AMAG Pharmaceuticals, Waltham, MA), used as an alternative contrast medium, is feasible in patients with impaired renal function. Other attractive imaging features of intravenous (IV) ferumoxytol include a prolonged blood pool phase and delayed intracellular uptake. With its unique pharmacological, metabolic and imaging properties, ferumoxytol may play a crucial role in future MR imaging of the central nervous system (CNS), various organs outside the CNS, and the cardiovascular system. Preclinical and clinical studies have demonstrated the overall safety and effectiveness of this novel contrast agent with rarely occurring anaphylactoid reactions. The purpose of this review is to describe the general and organ specific properties of ferumoxytol, as well as the advantages and potential pitfalls associated with its use in MRI. In order to more fully demonstrate the applications of ferumoxytol throughout the body, an imaging atlas was created and is available as supplementary material online.

Keywords

Introduction

Purpose of this review

Since the Food and Drug Administration (FDA) approved ferumoxytol (Feraheme, AMAG Pharmaceuticals, Waltham, MA) to treat iron deficiency anemia in adults with chronic kidney disease (CKD) in 2009, the off label use of this iron oxide nanoparticle compound by clinicians and researchers as a magnetic resonance imaging (MRI) contrast agent has grown

rapidly. Ferumoxytol-enhanced imaging is feasible in patients with impaired renal function, a patient population in whom both gadolinium and iodinated contrast agents are contraindicated. Other attractive imaging features of intravenous (IV) ferumoxytol include a prolonged blood pool phase and delayed intracellular uptake. Furthermore, since iron is a naturally occurring element in the body, the administered iron enters the body's natural iron metabolic pathways. Thus, the use of ferumoxytol is not currently associated with concerns regarding long-term deposition, as is the case with brain deposition of gadolinium-containing agents (1–4).

There are two aims of this review: first, to draw attention to a viable option of contrast enhanced cross sectional imaging in patients with renal failure; therefore *Kidney International* was chosen for publication. Second, to highlight the growing body of literature exploring a variety of clinical indications that suggest ferumoxytol may have utility not only as alternative to gadolinium-based contrast agents (GBCA), but also as a specialized MRI contrast agent with unique properties.

The number of clinical trials using ferumoxytol as a contrast agent is increasing. The co-authors are experienced in CNS, body or cardiovascular imaging with ferumoxytol. Based on the recommendations of the co-authors, we collected the relevant articles in the literature focusing on ferumoxytol over other ultrasmall superparamagnetic iron oxides (USPIOs) and highlighted the clinical applications rather than preclinical investigations.

This article describes ferumoxytol administration, dosing, and timing for imaging applications, followed by organ specific utilizations. We have created an atlas that more fully describes the application of ferumoxytol throughout the body and a table of relevant clinical publications using ferumoxytol which both can be found as an online supplement.

Ferumoxytol for iron replacement

Intravenous iron supplementation is important in patients with CKD owing to poor gastric absorption of oral iron. Insufficient absorption is related to the upregulation of hepcidin that occurs in CKD (5), which is exacerbated by excessive iron losses.

Though widely used, iron dextran, iron sucrose, and iron sodium gluconate have significant clinical limitations. Over the last decade, three new IV iron preparations have been developed that display tighter iron binding, allowing greater doses of iron to be given in a single administration. Along with ferric carboxymaltose and iron isomaltoside-1000, ferumoxytol has entered the therapeutic arena as an effective iron supplement (5). Ferumoxytol has favorable physicochemical characteristics, potentially reducing amounts of circulating free iron (6). Multiple studies have reported effective and safe treatment with ferumoxytol in iron deficiency (7–9).

Ferumoxytol for MR imaging

Initially, ferumoxytol was developed as an MRI contrast agent due to its effectiveness in shortening T1 and T2 relaxation times. Licensing the drug as a therapeutic iron supplement was likely a strategic decision, but this compound still holds great potential as an MRI contrast agent. Satisfactory contrast enhanced imaging can be performed with doses as low

as 1 mg/kg and as high as 510 mg total dose. See Figure 1 for the potential imaging phases following IV administration (Figure 1).

Arterial/venous dynamic phase—T2* based dynamic susceptibility contrast (DSC) perfusion imaging in the brain requires only 1 mg/kg ferumoxytol, and provides parametric maps in the brain similar to those achieved with a standard dose of gadolinium (10). The lack of early contrast extravasation with ferumoxytol is beneficial in cardiovascular and peripheral vascular examinations, wherein T1-weighted images acquired using a 4 mg/kg bolus injection clearly show intravascular enhancement as hyperintense structures. Although there is no evidence that these small bolus injections carry higher risk of adverse events, rapid injection of ferumoxytol is currently not recommended by the FDA (11).

Blood pool phase—One of the major advantages of nanoparticle imaging is the relatively long circulating time, with ferumoxytol displaying a plasma half-life of 14–21 h. Even in highly permeable tumors, high resolution imaging of the intravascular space can be achieved without visible background tissue enhancement. Steady-state blood volume mapping of the brain is a T2* based technique that requires 3–7 mg/kg ferumoxytol (12, 13), while the T1 based steady-state angiography of the peripheral vessels is performed using 3–4 mg/kg (14).

Delayed phase—In brain lesions, slow leakage of ferumoxytol through the disrupted blood-brain barrier (BBB) results in MRI signal changes peaking around 24 h after ferumoxytol administration (15). T1- weighted MRI shows signal increase similar to that seen with gadolinium. Signal decrease on T2/T2*- weighted images may represent high local iron concentration and/or intracellular uptake, which has many useful applications outside of the central nervous system (CNS). Indeed, intracellular uptake of ferumoxytol in abdominal organs, lymph nodes and vascular walls can be used to effectively delineate pathology in these areas (16, 17).

It is important to note that if a subsequent MRI is needed within 72 hours, ferumoxytol contrast enhancement may still be present in brain pathologies several days following administration. (15) In addition, decreased signal intensity in liver, spleen and bone marrow scans may persist for several months prior to returning to baseline.

Ferumoxytol metabolism and clearance

Following extravasation, ferumoxytol nanoparticles are taken up by cells of the mononuclear phagocyte system (MPS, previously known as reticuloendothelial system, RES), primarily in the liver, spleen and bone marrow. In the brain, macrophages or astrocytes contribute to ferumoxytol clearance (18, 19). Within these phagocytic cells, the nanoparticles are stored in secondary lysosomes (Figure 2) (19). The carboxymethyldextran coating is cleaved by dextranase and the cleaved coating is fully excreted by the kidneys and/or eliminated through feces. The iron core is incorporated into the body's iron stores and used for cell metabolism and hemoglobin synthesis. Unless the patient has known hemosiderosis or hemochromatosis, the administered iron during MRI examination (maximum 510 mg) is safe, and no overloading occurs (20).

Table 1 summarizes the physical, pharmacokinetic and imaging properties of ferumoxytol as compared to gadolinium.

Ferumoxytol safety

On March 30th, 2015, the FDA revised the prescribing information of Feraheme to include the addition of a boxed warning, which highlighted potential fatal and serious hypersensitivity reactions (HSR) including anaphylaxis. The warning emphasized the importance of trained personnel, appropriate medications being readily available, and monitoring patients for at least 30 minutes post administration to properly screen for HSR. In the three pre-marketing clinical trials of Feraheme (21–23) including 1164 patients, the aggregate rate of anaphylaxis was 0.2% (14). The post-marketing trials had even better results; the largest trial with 8666 patients showed a serious adverse events (SAE) rate of 0.2% and an anaphylaxis rate of 0.02% (24). Recently, several studies described the diagnostic use of ferumoxytol in the MRI suite and no SAEs were reported (20, 25–34). The frequency of ferumoxytol-related adverse events (10–14.6%) and SAEs (0–1%) were comparable in all investigations, with rates similar to those seen with ionic iodinated contrast agents, and were ten times higher than gadolinium-related events (35). The initial administration rate of a 510 mg bolus over 17 s was lowered to a slow infusion of 510 mg diluted ferumoxytol over 15 minutes as the FDA recommendation suggests. By reducing the rate of administration the frequency of these events may also be reduced.

Ferumoxytol has also shown an excellent safety profile in pediatric patients (20). Typical doses of 1–5 mg/kg for imaging purposes are much lower than the therapeutic dose and do not have a significant effect on hemoglobin values (20).

Central nervous system MR imaging with ferumoxytol

Table 2 and Figure 3 indicate the most commonly used imaging sequences in the CNS.

Intracranial neoplasms

The use of ferumoxytol in MRI of primary brain tumors has been extensively studied. While lesion visualization with ferumoxytol is generally similar to GBCAs, differences in enhancement patterns may help in differential diagnosis. Perfusion MRI and steady-state blood volume mapping may improve tumor grading by identifying the most malignant area for surgical targeting and therapy monitoring.

Lesion visualization—Contrast enhanced MRI is routinely performed for the diagnosis of brain tumors, where enhancement is the marker of BBB breakdown. Since extravasation of the large molecules is slow, parenchymal enhancement is best seen in the delayed phase, 24 h post ferumoxytol injection (15). Contrast enhancement is found on various clinically used T1-weighted MRI sequences, improves border delineation, and allows assessment of lesion internal morphology (36, 37) (Figure 4). In primary malignant brain tumors, contrast enhancement with ferumoxytol is comparable with GBCA enhancement. No significant difference was found in the number of enhancing masses when Gd-MRI and Fe-MRI were compared in various primary brain tumors and in metastatic lesions (38). Differences in

GBCA and ferumoxytol enhancement size and intensity may be present (37), and may reflect differences in pathology, contrast agent dose or timing of imaging. No difference was found in enhancement size with the two contrast agents in metastatic lesions (38) or in untreated glioma patients (36). Decreased signal on T2-weighted images in the delayed phase may indicate high local ferumoxytol concentration or retention in tumor-associated macrophages. Delayed T1 and T2 enhancement together may help differentiate extracellular iron (e.g. tumor necrosis) from intracellular iron (solid tumor) (39). T2*-weighted scans in the blood pool phase have a potential added value to standard of care by improving visualization of abnormal vasculature (40, 41).

Differential diagnosis—Dural-based enhancing masses may represent benign or malignant disease and there is no way to effectively distinguish between these pathologies solely with GBCA. Preliminary data suggests delayed T1 enhancement with ferumoxytol may help distinguish between meningioma and dural metastases when used in addition to GBCA. While all dural metastases enhanced strongly with ferumoxytol and GBCA, meningiomas showed poor to no enhancement with ferumoxytol (Figure 5) (42).

Tumefactive demyelinating lesions (TDLs) are large lesions usually accompanied by mass effect and abnormal enhancement, mimicking brain tumor, posing a particular diagnostic dilemma in patients with or without established diagnosis of multiple sclerosis (MS) (43). Definitive diagnosis is given after surgery and histopathological confirmation. A noninvasive marker is highly desirable to assess this diagnostic dilemma. Ferumoxytol uptake in inflammatory lesions appear on delayed T1- and T2-weighted images (44), furthermore perfusion MRI may help to differentiate tumors and demyelinating lesions with relative cerebral blood volume (rCBV) being lower in TDLs.

Blood volume based lesion assessment—Measurement of the blood volume in tissues can carry important information about the level of vascularization. Small molecular weight contrast agents can only estimate blood volume using dynamic first pass technique. An intravascular contrast agent allows measuring the blood volume using the steady-state technique, by calculating signal differences between pre- and post-contrast (intravascular) images. This has the benefit of high spatial resolution, since no rapid acquisition is necessary.

Dynamic susceptibility contrast perfusion-derived or steady-state CBV maps reflect brain tumor malignancy by revealing hypervascular, highly perfused tumor regions. rCBV (relative to normal reference region) has been shown to correlate with survival and facilitates preoperative diagnosis by differentiating low and high grade tumors (45). Moreover, elevated rCBV values can predict transformation of low grade gliomas into high grade tumors 12 months before T1 enhancement appears (46). Although these studies were performed using GBCA, ferumoxytol-derived rCBV values were in agreement with GBCA-derived values (10).

High grade gliomas, metastases, and to a lesser degree primary CNS lymphomas, exhibit high rCBV values with DSC or steady-state imaging, which can help differentiate them from demyelination, abscesses, and toxoplasmosis.

Intraoperative MRI and surgical targeting—More aggressive, hypervascular tumor regions with high rCBV values are the optimal sites for biopsy and can be identified using dynamic or steady-state perfusion imaging with ferumoxytol. Dynamic perfusion methods, however, have limited ability to differentiate between vessels and high tissue CBV, which compromises the assessment of small active tumor hotspots and could be the source of subsequent tumor progression and short survival. Due to its near distortion free high resolution images, steady-state CBV mapping can overcome this limitation and may enable more precise targeting (Figure 6). Late T2 enhancement with ferumoxytol has also been described to mark specific tumor areas and may again be useful for accurate biopsy targeting (44). Finally, delayed enhancement with ferumoxytol enables intra-and post-operative assessment of residual tumor without injecting additional contrast agent.

Treatment monitoring—After brain tumor therapy with radiation or chemoradiotherapy, increased edema and contrast enhancement on MRI may either represent tumor progression (growing tumor mass, indicating failure of ongoing therapy) or pseudoprogression, which is defined as a treatment-induced subacute inflammatory reaction without underlying tumor growth (47). Differentiating pseudoprogression from true tumor progression is a significant clinical problem. Response assessment according to the currently standard response assessment in neuro-oncology (RANO) criteria is based on morphology and contrast enhancement and may delay or prevent proper therapy (48). Similarly, antiangiogenic drugs affect BBB permeability without decreasing the tumor mass itself, which can lead to pseudoresponse (49) that cannot be differentiated from true response with the RANO criteria. It is becoming apparent that a phenomenon similar to pseudoprogression occurs after immune checkpoint blockade for cancer therapies (50). This has led to the development of immune-related response criteria to better identify cases of pseudoprogression (51), though these criteria are not specific to the CNS. According to the iRANO criteria published in 2015, patients who have imaging findings that meet RANO criteria for progressive disease within 6 months of starting immunotherapy should have a confirmation of follow up imaging (in 3 months) before defining the patients as non-responsive to treatment (52). The use of CBV mapping with ferumoxytol may help determine therapeutic efficacy in a variety of CNS tumors by differentiating highly vascular malignant tumor tissue from treatment related neuroinflammation, which correlates with survival (Figures 7 and 8) (10, 53).

We can now obtain high-resolution steady-state-CBV images that differentiate regions of high vascularity and active tumor growth (10, 13). Steady-state blood volume mapping with ferumoxytol is particularly helpful in imaging cortical lesions with improved spatial resolution.

Neuroinflammation and demyelination

Delayed imaging with ferumoxytol allows the assessment of inflammation as an imaging biomarker. Few human MS investigations are performed using ferumoxytol, but studies using other ultrasmall paramagnetic iron oxides (USPIO), such as ferumoxtran-10, have identified MS lesion phenotypes with the following enhancement patterns: 1. GBCA+/ delayed USPIO enhancement (USPIO+); 2. GBCA+/USPIO−; 3. GBCA−/USPIO+. The USPIO-specific lesions are of particular interest because they represent endothelial

activation and diapedesis without BBB disruption. Longitudinal studies demonstrate that in a fraction of GBCA−/USPIO+ MS lesions, delayed USPIO preceded GBCA enhancement by one month, suggesting extensive monocyte/macrophage extravasation in MS (54).

Ferumoxytol has been used to study neuroinflammatory processes associated with Japanese macaque encephalomyelitis (JME) (55), a demyelinating disease of the non-human primate with strong similarities to MS (56). A study by Tagge et al. demonstrated substantially greater USPIO+ lesion volume than GBCA+ lesion volume during the acute JME disease phase, indicating spatially and temporally extensive monocyte/macrophage migration into CNS (55).

Farrell et al. demonstrated delayed enhancement with ferumoxytol in patients with MS, primary CNS lymphoma, posttransplant lymphoproliferative disorder, acute disseminated encephalomyelitis (ADEM) (Figure 9) (44) and chronic encephalitis; a higher number of lesions are visible with ferumoxytol, than with GBCAs.

Future applications (ultrahigh field MRI, seizure imaging, functional MRI and vascular imaging in the CNS) can be found in the online supplement.

Body imaging with ferumoxytol

Liver and spleen

Metastases are the most common solid liver lesions (though benign hepatic hemangiomas are also frequent) and MRI is considered the definitive tool for differentiating these entities in the oncologic setting. However, this task can be difficult when lesions are small or when hemangiomas are atypical or of the sclerosing subtype. In many cases, small hemangiomas can be differentiated from other lesions based on retention of intravascular contrast agents such as gadofosveset trisodium or ferumoxytol on delayed scans (57, 58).

Significant negative (hypointense) T2 enhancement of normal liver parenchyma is seen within 10 min of IV ferumoxytol administration. Since ferumoxytol is taken up by the MPS, it has the potential to serve as a tool for measuring MPS dysfunction. Quantitative measures of MPS function, as estimated from dynamic imaging of ferumoxytol uptake in the liver, may prove to be useful predictors of graft dysfunction and rejection, although validations in humans are still pending (59).

Pancreas

CT is the imaging method of choice for pancreatic diseases including pancreatic adenocarcinoma, pancreatitis and neuroendocrine tumors of the pancreas. Imaging of the pancreas with MRI holds significant promise secondary to the many inherent contrast mechanisms, particularly with novel contrast agents.

Blood vessel density is known to be markedly lower in pancreatic ductal adenocarcinoma (PDAC) compared with other malignancies (60), which may explain its poor response to anti-angiogenic therapies, and makes PDAC a poor choice for interrogation with dynamic techniques. Because of the long intravascular blood pool residence time, iron oxide

nanoparticles offer a steady-state solution for precise measurements of microvascular parameters as demonstrated in preclinical studies (61–64) and are better imaging agents for PDAC. In subcutaneous xenograft models, MRI of magnetic nanoparticles provides a non-invasive, accurate assessment of fractional blood volume and vessel size index (62–72).

The delayed uptake of magnetic nanoparticles by macrophages (73) has also been a focus of MRI for multiple applications in the pancreas as well, including improved delineation of pancreatic adenocarcinoma (17) and for quantifying inflammation in patients with early onset type I diabetes (Figure 11) (74, 75).

Staging of malignant tumors

The current anatomic imaging techniques for nodal staging (e.g. CT, MRI) rely on morphologic lymph node characteristics such as size, shape and morphology, but sensitivity for differentiating malignant from benign lymph nodes remains low (76). Sensitivity could be improved using USPIO, however, most of the available data have been obtained with USPIOs other than ferumoxytol (77, 78). Iron oxide particles are taken up by and retained in normal lymph nodes, resulting in signal loss on T2- and T2*- weighted images (Figure 12) (79). When nodes are infiltrated with malignant cells, nodal USPIO nanoparticle uptake capacity reduces and malignant nodes retain high signal intensity on T2*-weighted images. Optimal node T2*-weighted imaging contrast with ferumoxytol can be achieved 24–48 h post-injection (Figures 12 and 13) (16, 79).

Prostate—Nodal involvement is noted in 5% to 10% of patients with prostate carcinoma, but CT and MR detection sensitivity remains lower than 30% (80).

Clinical experience with ferumoxytol-enhanced MRI for mapping metastatic lymph nodes in patients with prostate cancer is limited. Harisinghani et al. (16) reported a significant drop in the SNR in benign nodes on T2*-weighted images, but little change in SNR in malignant nodes using ferumoxytol at a dose of 4 mg/kg. MRI was performed before, 5, 18, and 24 hours after ferumoxytol injection. The most appropriate dose of ferumoxytol is uncertain as lymph nodes in the pelvis are heterogeneous. Turkbey et al. found that a higher dose of IV ferumoxytol (up to 7.5 mg/kg) is needed to completely darken normal pelvic nodes compared to ferumoxtran-10 (81).

Direct injection of ferumoxytol into the prostate (lymphography) has shown promise in mapping sentinel lymph nodes, as demonstrated in non-human primates (82).

Other potential applications in body imaging (breast and sentinel lymph node, colorectal-, adrenal gland MRI and stem cell labeling) can be found in the online supplement.

Inflammation

Focal inflammation can mimic neoplasia. By labeling macrophages with ferumoxytol in vivo, macrophage trafficking can be detected and inflammatory lesions can be localized (83, 84).

Ferumoxytol-enhanced MRI is promising for assessing rheumatologic diseases and differentiating acute from chronic inflammatory kidney disease (85–88). Ferumoxytol-enhanced MRI has also been used for diagnosing osteomyelitis in the feet of patients with diabetes (Figure 14) (89) as well as detecting the activity of Crohn's disease (90).

Pediatric MR imaging with ferumoxytol

Using ferumoxytol as an MR imaging agent in the pediatric population has similar potential benefits as in adults. Specific advantages include separation of IV cannula placement/ferumoxytol administration from the MRI scanning itself (which may improve the cooperation of the child if MRI is performed without anesthesia) (32). For pediatric brain tumor patients, undergoing MRI with anesthesia, gadolinium and ferumoxytol in a single imaging session was well tolerated (33). 3D contrast enhanced MRA applications in pediatric patients with CKD have been reported to evaluate IV access placement, vascular thrombosis, cardiac and renal transplantation anastomosis, re-transplantation or biliary/liver dysfunction, eliminating concerns about nephrogenic systemic fibrosis (30, 91). Finally, ferumoxytol may provide a higher level of confidence for the delineation of small vessels prior to surgery in body MRA (32).

Many types of lymphomas, soft tissue sarcomas and bone sarcomas are staged with 18F-FDG-PET/CT (92). In order to provide a radiation free alternative, whole body diffusion-weighted MR (WB-DW MR) imaging has been developed without the use of contrast agents. However, the use of ferumoxytol with this technique may be advantageous(Figure 15) (28).

Vascular MR imaging with ferumoxytol

For contrast enhanced MRA, MR users have traditionally employed timed, first pass imaging of a gadolinium bolus, focused on the arterial or venous territory of interest. For the majority of GBCA, the volume of distribution is the extracellular fluid space and this is assessed quickly after the arterial first pass. The time window for a pure or predominantly vascular phase is therefore very short and the acquisition can be technically challenging. Gadofosveset is the one GBCA with an extended blood residence time due to reversible binding to serum albumin. However, compared to ferumoxytol, gadofosveset has a much shorter intravascular half-life (30 min vs 14–21 h) and at any given time, ~20% is distributed in the extracellular fluid space. Moreover, gadofosveset is being withdrawn from production such that by the end of 2016, ferumoxytol will be the only intravascular MRI contrast agent available for human use in the U.S.

Patients with vascular disease are a challenging group for imaging; many (20–30%) are diabetic with associated difficult vein access (93) and many (20–40%) have CKD, which can prohibit the use of iodine-and gadolinium-based contrast agents (34, 94). Ferumoxytol is a very attractive option in these patients and it can be used without the need for bolus timing or complex image acquisition schemes. Ferumoxytol's excellent safety profile has already been established in patients with chronic renal insufficiency, though it must always be used with close physiological monitoring.

In recent years, there have been several reports of the successful use of ferumoxytol for vascular imaging in adults and children with renal failure (30, 32, 34, 57, 91, 95, 96). The studies suggest that ferumoxytol provides similar or improved quality images compared to GBCAs, without the concerns of long term gadolinium accumulation (1–4). Some of the potential applications for ferumoxytol in vascular imaging are summarized in Table 3.

Cardiac imaging

To date, there have been very few reports of the use of ferumoxytol in patients with ischemic heart disease. In patients with acute myocardial infarction, Alam et al. (97) and Yilmaz et al. (98) showed macrophage activation in injured myocardium. These authors exploited the effects of ferumoxytol in causing signal loss due to its effect on T2 values and did not address vascular enhancement due to shortening of T1 values.

In congenital heart disease, accurate anatomical assessment is important for surgical or interventional planning. Conventional first pass MRA and 2D cardiac cine methods provide limited definition of intracardiac structures. On the other hand, ferumoxytol supports the acquisition of 4-dimensional images of the beating heart with Four-Dimensional, Multiphase, Steady-State Imaging with Contrast Enhancement (MUSIC) (Figure 16) (99). Similarly, comprehensive motion-compensated highly accelerated 4D flow MRI with ferumoxytol enhances the quality of 4-dimensional flow information with reduced respiratory motion artifacts in children with congenital heart disease (100, 101).

The imaging goals for most congenital heart diseases include quantification of blood flow in the great vessels, determination of cardiac chamber volumes and contractility, and assessment of segmental anatomy. Typically, this requires a lengthy MRI scan with over an hour of repeated breath holding under anesthesia with specialized technologists and physicians on hand to prescribe customized planes for image acquisition. A compelling advantage of ferumoxytol is that it enables volumetric temporally-resolved high resolution imaging without breath holding (99). Further, a free-breathing volumetric comprehensive MRI yielding flow, function, and anatomic assessment in less than 10 min has been achieved (100). Additionally, ventricular mass may be quantified with this same technique (101). As a result, no special operator knowledge of cardiac anatomy is required, and the duration of anesthesia and complexity of the procedure for congenital heart MRI can be greatly reduced. These techniques stand to revolutionize the approach to MR imaging of children with complex congenital heart diseases.

Aortic imaging

Aortic imaging can be performed with a computed tomography angiography (CTA), non-contrast MRI or gadolinium enhanced MRA. Blood volume, flow measurements, and morphological assessments can be made with contrast enhanced MRA using a combination of time-resolved and steady-state images. Inflammation in the aortic wall can potentially be assessed using in vivo macrophage labeling with ferumoxytol, which is not available with gadolinium-enhanced imaging. Inflammation plays a key role in the progression and vulnerability to rupture of atherosclerotic plaques in many arterial territories. The presence of inflammation can also predict vessel patency (102, 103).

Additionally, due to its long intravascular half-life, ferumoxytol can be used for the detection of aortic endoleaks after endovascular aneurysm repair. A systematic review showed that MRA detected almost twice as many endoleaks as CTA (104). Iron oxide-enhanced MRA (either with ferumoxytol or with ferucarbotran) may be advantageous for demonstrating endoleaks (105, 106).

Visceral arteries and arteriovenous (AV) fistulas

Patients with end-organ ischemia in the abdominal vasculature often have diabetes and renal insufficiency. Ferumoxytol may therefore be a useful agent for assessing renal artery stenosis, pre- and post-transplantation vessel patency, and for new venous access. In pre and post renal and liver transplantation patients, ferumoxytol has been used to assess vascular integrity (30, 95). The frequent occurrence of venous occlusion in these patients, and the requirement to confirm or re-establish venous access, makes high resolution venous imaging with ferumoxytol invaluable (Figure 17) (91).

Most studies regarding pre-fistula assessments involve pediatric patients, since this group benefits the most from ferumoxytol-enhanced MRA. In a feasibility study using ferumoxytol for clinical pediatric cardiovascular imaging, Ruanwattanapaisarn et al. evaluated renal transplant or post-transplant complications, vascular shunts, stenosis, aneurysms and congenital heart disease, and found excellent image quality of the hepatic arteries, superior mesenteric artery, renal arteries, pulmonary arteries, pulmonary veins, valves and ventricles (32). Ferumoxytol-enhanced MRA provided consistently superior quality TOF MRA images in patients with AV fistulas (96).

Other applications in vascular imaging (carotid-, peripheral artery imaging and magnetic resonance venography) can be found in the online supplement.

Discussion

In this review, we draw attention to ferumoxytol as a contrast agent for cross sectional imaging in patients with renal failure and highlighted the variety of clinical indications in which ferumoxytol may not only be an alternative to GBCA, but also a specialized contrast agent with unique properties. These include the extended blood pool phase, and uptake into the MPS in the delayed phase, where nanoparticles are metabolized as iron.

Ferumoxytol has been approved by the FDA for iron replacement in 2009, and it is available for off label clinical use. A large and growing body of literature has been reviewed in this manuscript showing potentials of ferumoxytol imaging. Although most available evidence is based on single center studies, pilot studies, retrospective analyses or preclinical results, there are new multicenter, multiplatform studies being designed (clinicaltrials.gov, NCT02359097). Application for FDA approval of using ferumoxytol as an imaging agent is in preparation, which would further ease its widespread use of ferumoxytol in MR imaging.

Limitations

Besides known hypersensitivity or iron metabolic disorders, there is no absolute contraindication of ferumoxytol for MR imaging, and importantly is safe in patients with

renal impairment. Vascular visualization improves early after administration, while late enhancement visualizes parenchymal/intracellular enhancement, which may require an additional visit, posing a logistical limitation with MRI scheduling. Signal change in the brain may persist from a few days to a week. Uptake in the liver, spleen and bone marrow may alter MRI signal for months, therefore, radiologists must be aware of prior history of IV iron oxide use. While hypersensitivity reactions occur, the incidence of serious ferumoxytol rela1ted hypersensitivity is very low and new FDA guidelines aim to further improve patient safety.

Conclusion

In conclusion, there are numerous potential applications of ferumoxytol for MRI throughout the body, including the CNS, various organs outside of the CNS, and the cardiovascular system. Whether used where GBCA is contraindicated, or for applications that are currently outside the scope of GBCA, ferumoxytol has shown sufficient promise to warrant vigorous research into its ultimate clinical role. Radiological modalities which are noninvasive, radiation free and safe are generally preferred and should be further developed; ferumoxytol MRI may be an important step in this direction.

Supplementary Material

Refer to Web version on PubMed Central for supplementary material.

Acknowledgments

References

1. Kanda T, Oba H, Toyoda K, Kitajima K, Furui S. Brain gadolinium deposition after administration of gadolinium-based contrast agents. Japanese journal of radiology. 2016; 34(1):3–9. [PubMed: 26608061]

2. Ramalho J, Semelka RC, AlObaidy M, Ramalho M, Nunes RH, Castillo M. Signal intensity change on unenhanced T1-weighted images in dentate nucleus following gadobenate dimeglumine in patients with and without previous multiple administrations of gadodiamide. European radiology. 2016

3. Reeder SB, Gulani V. Gadolinium Deposition in the Brain: Do We Know Enough to Change Practice? Radiology. 2016; 279(1):323–6.

4. Stojanov D, Aracki-Trenkic A, Benedeto-Stojanov D. Gadolinium deposition within the dentate nucleus and globus pallidus after repeated administrations of gadolinium-based contrast agents-current status. Neuroradiology. 2016; 58(5):433–41. [PubMed: 26873830]

5. Kowalczyk M, Banach M, Rysz J. Ferumoxytol: a new era of iron deficiency anemia treatment for patients with chronic kidney disease. Journal of nephrology. 2011; 24(6):717–22. [PubMed: 21956770]

6. Balakrishnan VS, Rao M, Kausz AT, Brenner L, Pereira BJ, Frigo TB, et al. Physicochemical properties of ferumoxytol, a new intravenous iron preparation. European journal of clinical investigation. 2009; 39(6):489–96. [PubMed: 19397688]

7. Hetzel D, Strauss W, Bernard K, Li Z, Urboniene A, Allen LF. A Phase III, randomized, open-label trial of ferumoxytol compared with iron sucrose for the treatment of iron deficiency anemia in patients with a history of unsatisfactory oral iron therapy. American journal of hematology. 2014; 89(6):646–50. [PubMed: 24639149]

8. Macdougall IC, Strauss WE, McLaughlin J, Li Z, Dellanna F, Hertel J. A randomized comparison of ferumoxytol and iron sucrose for treating iron deficiency anemia in patients with CKD. Clinical journal of the American Society of Nephrology : CJASN. 2014; 9(4):705–12. [PubMed: 24458078]

9. Vadhan-Raj S, Ford DC, Dahl NV, Bernard K, Li Z, Allen LF, et al. Safety and efficacy of ferumoxytol for the episodic treatment of iron deficiency anemia in patients with a history of unsatisfactory oral iron therapy: Results of a phase III, open-label, 6-month extension study. American journal of hematology. 2016; 91(2):E3–5. [PubMed: 26572233]

10. Gahramanov S, Muldoon LL, Varallyay CG, Li X, Kraemer DF, Fu R, et al. Pseudoprogression of glioblastoma after chemo- and radiation therapy: diagnosis by using dynamic susceptibility-weighted contrast-enhanced perfusion MR imaging with ferumoxytol versus gadoteridol and correlation with survival. Radiology. 2013; 266(3):842–52. [PubMed: 23204544]

11. FDA Drug Safety Communication. FDA strengthens warnings and changes prescribing instructions to decrease the risk of serious allergic reactions with anemia drug Feraheme (ferumoxytol). 2015

12. Christen T, Ni W, Qiu D, Schmiedeskamp H, Bammer R, Moseley M, et al. High-resolution cerebral blood volume imaging in humans using the blood pool contrast agent ferumoxytol. Magnetic resonance in medicine. 2013; 70(3):705–10. [PubMed: 23001902]

13. Varallyay CG, Nesbit E, Fu R, Gahramanov S, Moloney B, Earl E, et al. High-resolution steady-state cerebral blood volume maps in patients with central nervous system neoplasms using ferumoxytol, a superparamagnetic iron oxide nanoparticle. J Cereb Blood Flow Metab. 2013; 33(5):780–6. [PubMed: 23486297]

14. Finn JP, Nguyen KL, Han F, Zhou Z, Salusky I, Ayad I, et al. Cardiovascular MRI with ferumoxytol. Clinical radiology. 2016; 71(8):796–806. [PubMed: 27221526]

15. Neuwelt EA, Varallyay CG, Manninger S, Solymosi D, Haluska M, Hunt MA, et al. The potential of ferumoxytol nanoparticle magnetic resonance imaging, perfusion, and angiography in central nervous system malignancy: a pilot study. Neurosurgery. 2007; 60(4):601–11. discussion 11–2. [PubMed: 17415196]

16. Harisinghani M, Ross RW, Guimaraes AR, Weissleder R. Utility of a new bolus-injectable nanoparticle for clinical cancer staging. Neoplasia (New York, NY). 2007; 9(12):1160–5.

17. Hedgire S, Mino-Kenudson M, Elmi A, Thayer S, Fernandez-del Castillo C, Harisinghani M. Enhanced primary tumor delineation in pancreatic adenocarcinoma using ultrasmall super paramagnetic iron oxide nanoparticle-ferumoxytol: an initial experience with histopathologic correlation. Int J Nanomedicine. 2014; 9:1891–6. [PubMed: 24790431]

18. Daldrup-Link HE, Golovko D, Ruffell B, Denardo DG, Castaneda R, Ansari C, et al. MRI of tumor-associated macrophages with clinically applicable iron oxide nanoparticles. Clin Cancer Res. 2011; 17(17):5695–704. [PubMed: 21791632]

19. McConnell HL, Schwartz DL, Richardson BE, Woltjer RL, Muldoon LL, Neuwelt EA. Ferumoxytol nanoparticle uptake in brain during acute neuroinflammation is cell-specific. Nanomedicine : nanotechnology, biology, and medicine. 2016

20. Muehe AM, Feng D, von Eyben R, Luna-Fineman S, Link MP, Muthig T, et al. Safety Report of Ferumoxytol for Magnetic Resonance Imaging in Children and Young Adults. Investigative radiology. 2016; 51(4):221–7. [PubMed: 26656202]

21. Provenzano R, Schiller B, Rao M, Coyne D, Brenner L, Pereira BJ. Ferumoxytol as an intravenous iron replacement therapy in hemodialysis patients. Clin J Am Soc Nephrol. 2009; 4(2):386–93. [PubMed: 19176796]

22. Singh A, Patel T, Hertel J, Bernardo M, Kausz A, Brenner L. Safety of ferumoxytol in patients with anemia and CKD. American journal of kidney diseases : the official journal of the National Kidney Foundation. 2008; 52(5):907–15. [PubMed: 18824288]

23. Spinowitz BS, Kausz AT, Baptista J, Noble SD, Sothinathan R, Bernardo MV, et al. Ferumoxytol for treating iron deficiency anemia in CKD. Journal of the American Society of Nephrology : JASN. 2008; 19(8):1599–605. [PubMed: 18525001]

24. Schiller B, Bhat P, Sharma A. Safety and effectiveness of ferumoxytol in hemodialysis patients at 3 dialysis chains in the United States over a 12-month period. Clinical therapeutics. 2014; 36(1):70–83. [PubMed: 24315802]

25. Bashir MR, Mody R, Neville A, Javan R, Seaman D, Kim CY, et al. Retrospective assessment of the utility of an iron-based agent for contrast-enhanced magnetic resonance venography in patients with endstage renal diseases. Journal of magnetic resonance imaging : JMRI. 2014; 40(1):113–8. [PubMed: 24130008]

26. D'Arceuil H, Coimbra A, Triano P, Dougherty M, Mello J, Moseley M, et al. Ferumoxytol enhanced resting state fMRI and relative cerebral blood volume mapping in normal human brain. NeuroImage. 2013; 83:200–9. [PubMed: 23831413]

27. Hasan DM, Amans M, Tihan T, Hess C, Guo Y, Cha S, et al. Ferumoxytol-enhanced MRI to Image Inflammation within Human Brain Arteriovenous Malformations: A Pilot Investigation. Translational stroke research. 2012; 3(Suppl 1):166–73. [PubMed: 23002401]

28. Klenk C, Gawande R, Uslu L, Khurana A, Qiu D, Quon A, et al. Ionising radiation-free whole-body MRI versus (18)F-fluorodeoxyglucose PET/CT scans for children and young adults with cancer: a prospective, non-randomised, single-centre study. Lancet Oncol. 2014; 15(3):275–85. [PubMed: 24559803]

29. Li W, Tutton S, Vu AT, Pierchala L, Li BS, Lewis JM, et al. First-pass contrast-enhanced magnetic resonance angiography in humans using ferumoxytol, a novel ultrasmall superparamagnetic iron oxide (USPIO)-based blood pool agent. Journal of magnetic resonance imaging : JMRI. 2005; 21(1):46–52. [PubMed: 15611942]

30. Nayak AB, Luhar A, Hanudel M, Gales B, Hall TR, Finn JP, et al. High-resolution, whole-body vascular imaging with ferumoxytol as an alternative to gadolinium agents in a pediatric chronic kidney disease cohort. Pediatric nephrology (Berlin, Germany). 2015; 30(3):515–21.

31. Ning P, Zucker EJ, Wong P, Vasanawala SS. Hemodynamic safety and efficacy of ferumoxytol as an intravenous contrast agents in pediatric patients and young adults. Magnetic resonance imaging. 2016; 34(2):152–8. [PubMed: 26518061]

32. Ruangwattanapaisarn N, Hsiao A, Vasanawala SS. Ferumoxytol as an off-label contrast agent in body 3T MR angiography: a pilot study in children. Pediatric radiology. 2015; 45(6):831–9. [PubMed: 25427433]

33. Thompson EM, Guillaume DJ, Dosa E, Li X, Nazemi KJ, Gahramanov S, et al. Dual contrast perfusion MRI in a single imaging session for assessment of pediatric brain tumors. Journal of neuro-oncology. 2012; 109(1):105–14. [PubMed: 22528798]

34. Walker JP, Nosova E, Sigovan M, Rapp J, Grenon MS, Owens CD, et al. Ferumoxytol-enhanced magnetic resonance angiography is a feasible method for the clinical evaluation of lower extremity arterial disease. Ann Vasc Surg. 2015; 29(1):63–8. [PubMed: 25269682]

35. Vasanawala SS, Nguyen KL, Hope MD, Bridges MD, Hope TA, Reeder SB, et al. Safety and technique of ferumoxytol administration for MRI. Magnetic resonance in medicine. 2016; 75(5):2107–11. [PubMed: 26890830]

36. Hamilton BE, Nesbit GM, Dosa E, Gahramanov S, Rooney B, Nesbit EG, et al. Comparative analysis of ferumoxytol and gadoteridol enhancement using T1- and T2-weighted MRI in neuroimaging. AJR American journal of roentgenology. 2011; 197(4):981–8. [PubMed: 21940589]

37. Dosa E, Guillaume DJ, Haluska M, Lacy CA, Hamilton BE, Njus JM, et al. Magnetic resonance imaging of intracranial tumors: intra-patient comparison of gadoteridol and ferumoxytol. Neuro Oncol. 2011; 13(2):251–60. [PubMed: 21163809]

38. Hamilton, BEN.GMBarajas, R.Ambrady, P., Neuwelt, EA., editors. Ferumoxytol enhanced MRI detection of brain metastatic disease. ASNR; Washington DC: 2016.

39. Aghighi M, Golovko D, Ansari C, Marina NM, Pisani L, Kurlander L, et al. Imaging Tumor Necrosis with Ferumoxytol. PloS one. 2015; 10(11):e0142665. [PubMed: 26569397]

40. Dosa E, Tuladhar S, Muldoon LL, Hamilton BE, Rooney WD, Neuwelt EA. MRI using ferumoxytol improves the visualization of central nervous system vascular malformations. Stroke. 2011; 42(6):1581–8. [PubMed: 21493906]

41. Neuwelt EA, Hamilton BE, Varallyay CG, Rooney WR, Edelman RD, Jacobs PM, et al. Ultrasmall superparamagnetic iron oxides (USPIOs): a future alternative magnetic resonance (MR) contrast agent for patients at risk for nephrogenic systemic fibrosis (NSF)? Kidney Int. 2009; 75(5):465–74. [PubMed: 18843256]

42. Hamilton BE, Woltjer RL, Prola-Netto J, Nesbit GM, Gahramanov S, Pham T, et al. Ferumoxytol-enhanced MRI differentiation of meningioma from dural metastases: a pilot study with immunohistochemical observations. J Neurooncol. 2016

43. Abdoli M, Freedman MS. Neuro-oncology dilemma: Tumour or tumefactive demyelinating lesion. Multiple sclerosis and related disorders. 2015; 4(6):555–66. [PubMed: 26590662]

44. Farrell BT, Hamilton BE, Dosa E, Rimely E, Nasseri M, Gahramanov S, et al. Using iron oxide nanoparticles to diagnose CNS inflammatory diseases and PCNSL. Neurology. 2013; 81(3):256–63. [PubMed: 23771486]

45. Law M, Yang S, Wang H, Babb JS, Johnson G, Cha S, et al. Glioma grading: sensitivity, specificity, and predictive values of perfusion MR imaging and proton MR spectroscopic imaging compared with conventional MR imaging. AJNR American journal of neuroradiology. 2003; 24(10):1989–98. [PubMed: 14625221]

46. Danchaivijitr N, Waldman AD, Tozer DJ, Benton CE, Brasil Caseiras G, Tofts PS, et al. Low-grade gliomas: do changes in rCBV measurements at longitudinal perfusion-weighted MR imaging predict malignant transformation? Radiology. 2008; 247(1):170–8. [PubMed: 18372467]

47. Brandsma D, Stalpers L, Taal W, Sminia P, van den Bent MJ. Clinical features, mechanisms, and management of pseudoprogression in malignant gliomas. Lancet Oncol. 2008; 9(5):453–61. [PubMed: 18452856]

48. Nasseri M, Gahramanov S, Netto JP, Fu R, Muldoon LL, Varallyay C, et al. Evaluation of pseudoprogression in patients with glioblastoma multiforme using dynamic magnetic resonance imaging with ferumoxytol calls RANO criteria into question. Neuro Oncol. 2014; 16(8):1146–54. [PubMed: 24523362]

49. Varallyay CG, Muldoon LL, Gahramanov S, Wu YJ, Goodman JA, Li X, et al. Dynamic MRI using iron oxide nanoparticles to assess early vascular effects of antiangiogenic versus corticosteroid treatment in a glioma model. J Cereb Blood Flow Metab. 2009; 29(4):853–60. [PubMed: 19142191]

50. Cohen JV, Alomari AK, Vortmeyer AO, Jilaveanu LB, Goldberg SB, Mahajan A, et al. Melanoma Brain Metastasis Pseudoprogression after Pembrolizumab Treatment. Cancer Immunol Res. 2016; 4(3):179–82. [PubMed: 26701266]

51. Hodi FS, Hwu WJ, Kefford R, Weber JS, Daud A, Hamid O, et al. Evaluation of Immune- Related Response Criteria and RECIST v1.1 in Patients With Advanced Melanoma Treated With Pembrolizumab. J Clin Oncol. 2016; 34(13):1510–7. [PubMed: 26951310]

52. Okada H, Weller M, Huang R, Finocchiaro G, Gilbert MR, Wick W, et al. Immunotherapy response assessment in neuro-oncology: a report of the RANO working group. Lancet Oncol. 2015; 16(15):e534–42. [PubMed: 26545842]

53. Gahramanov S, Varallyay C, Tyson RM, Lacy C, Fu R, Netto JP, et al. Diagnosis of pseudoprogression using MRI perfusion in patients with glioblastoma multiforme may predict improved survival. CNS Oncol. 2014; 3(6):389–400. [PubMed: 25438810]

54. Vellinga MM, Oude Engberink RD, Seewann A, Pouwels PJ, Wattjes MP, van der Pol SM, et al. Pluriformity of inflammation in multiple sclerosis shown by ultra-small iron oxide particle enhancement. Brain : a journal of neurology. 2008; 131(Pt 3):800–7. [PubMed: 18245785]

55. Tagge. A Comparative Volumetric Study in Acute Japanese Macaque Encephalomyelitis. Proc Int Soc Magn Reson Med. 2015

56. Axthelm MK, Bourdette DN, Marracci GH, Su W, Mullaney ET, Manoharan M, et al. Japanese macaque encephalomyelitis: a spontaneous multiple sclerosis-like disease in a nonhuman primate. Annals of neurology. 2011; 70(3):362–73. [PubMed: 21674589]

57. Bashir MR, Bhatti L, Marin D, Nelson RC. Emerging applications for ferumoxytol as a contrast agent in MRI. Journal of magnetic resonance imaging : JMRI. 2015; 41(4):884–98. [PubMed: 24974785]

58. Milot L, Haider M, Foster L, McGregor C, Law C. Gadofosveset trisodium in the investigation of focal liver lesions in noncirrhotic liver: Early experience. Journal of magnetic resonance imaging : JMRI. 2012; 36(3):738–42. [PubMed: 22488745]

59. Liu T, Choi H, Zhou R, Chen IW. Quantitative evaluation of the reticuloendothelial system function with dynamic MRI. PloS one. 2014; 9(8):e103576. [PubMed: 25090653]

60. Olive K, Jacobetz M, Davidson C, Gopinathan A, McIntyre D, Honess D, et al. Inhibition of Hedgehog signaling enhances delivery of chemotherapy in a mouse model of pancreatic cancer. Science. 2009; 324(5933):1457–61. [PubMed: 19460966]

61. Boxerman J, Hamberg L, Rosen B, Weisskoff R. MR contrast due to intravascular magnetic susceptibility perturbations. Magnetic resonance in medicine. 1995; 34(4):555–66. [PubMed: 8524024]

62. Bremer C, Mustafa M, Bogdanov A Jr, Petrovsky A, Weissleder R. Steady-state blood volume measurements in Experimental tumors with different angiogenic burdens - a study in mice. Radiology. 2003; 226(1):214–20. [PubMed: 12511693]

63. Dennie J, Mandeville J, Boxerman J, Packard S, Rosen B, Weisskoff R. NMR imaging of changes in vascular morphology due to tumor angiogenesis. Magnetic resonance in medicine. 1998; 40:793–99. [PubMed: 9840821]

64. Guimaraes A, Rakhlin E, Weissleder R, Thayer S. Magnetic resonance imaging monitors physiological changes with antihedgehog therapy in pancreatic adenocarcinoma xenograft model. Pancreas. 2008; 37(4):440–4. [PubMed: 18953259]

65. CTF, WSK, CDL, YRK, SJK, GD, et al. In Vivo validation of MRI vessel caliber index measurement methods with intravital optical microscopy in a u87 mouse brain tumor. Neuro Oncology. 2010 In Press.

66. Emblem K, Farrar C, Gerstner E, Batchelor T, Borra R, Rosen B, et al. Vessel caliber--a potential MRI biomarker of tumour response in clinical trials. Nat Rev Clin Oncol. 2014; 11(10):566–84. [PubMed: 25113840]

67. Flexman, J., Yung, A., Yapp, D., Ng, S., Kozlowski, P. Assessment of Vessel Size by MRI in Orthotopic Model of Human Pancreatic Cancer. Annual International IEEE EMBS Conference; 2009; Vancouver, BC, Canada. p. 851-4.

68. Guimaraes A, Ross R, Figuereido J, Waterman P, Weissleder R. MRI with magnetic nanoparticles monitors downstream anti-angiogenic effects of mTOR inhibition. Mol Imaging Biol. 2011; 13(2): 314–20. [PubMed: 20559742]

69. Jensen J, Chandra R. MR imaging of microvasculature. Magnetic resonance in medicine. 2000; 44(2):224–30. [PubMed: 10918321]

70. Kiselev V, Strecker R, Ziyeh S, Speck O, Hennig J. Vessel size imaging in humans. Magnetic resonance in medicine. 2005; 53(3):553–63. [PubMed: 15723391]

71. Lemasson B, Valable S, Farion R, Krainik A, Remy C, Barbier E. In vivo imaging of vessel diameter, size, and density: a comparative study between MRI and histology. Magnetic resonance in medicine. 2013; 69(1):18–26. [PubMed: 22431289]

72. Tropres I, Grimault S, Vaeth A, Grillon E, Julien C, Payen J, et al. Vessel size imaging. Magnetic resonance in medicine. 2001; 45:397–408. [PubMed: 11241696]

73. Weissleder R, Elizaondo G, Wittenberg J, et al. Ultrasmall superparamagnetic iron oxide: characterization of a new class of contrast agents for MR imaging. Radiology. 1990; 175:489–93. [PubMed: 2326474]

74. Gaglia J, Guimaraes A, Harisinghani M, Turvey S, Jackson R, Benoist C, et al. Noninvasive imaging of pancreatic islet inflammation in type 1A diabetes patients. J Clin Invest. 2011; 121(1): 442–5. [PubMed: 21123946]

75. Gaglia J, Harisinghani M, Aganj I, Wojtkiewicz G, Hedgire S, Benoist C, et al. Noninvasive mapping of pancreatic inflammation in recent-onset type-1 diabetes patients. Proc Natl Acad Sci U S A. 2015; 112(7):2139–44. [PubMed: 25650428]

76. Ganeshalingam S, Koh D-M. Nodal staging. Cancer Imaging. 2009; 9(1):104–11. [PubMed: 20080453]

77. Barentsz J. MR imaging of pelvic lymph nodes. Cancer Imaging. 2003; 3(2):130–4.

78. Harisinghani MG, Saini S, Slater GJ, Schnall MD, Rifkin MD. MR imaging of pelvic lymph nodes in primary pelvic carcinoma with ultrasmall superparamagnetic iron oxide (Combidex): preliminary observations. Journal of magnetic resonance imaging : JMRI. 1997; 7(1):161–3. [PubMed: 9039609]

79. Anzai Y, Piccoli CW, Outwater EK, Stanford W, Bluemke DA, Nurenberg P, et al. Evaluation of neck and body metastases to nodes with ferumoxtran 10-enhanced MR imaging: phase III safety and efficacy study. Radiology. 2003; 228(3):777–88. [PubMed: 12954896]

80. Wolf JS Jr, Cher M, Dall'era M, Presti JC Jr, Hricak H, Carroll PR. The use and accuracy of cross-sectional imaging and fine needle aspiration cytology for detection of pelvic lymph node metastases before radical prostatectomy. The Journal of urology. 1995; 153(3 Pt 2):993–9. [PubMed: 7853590]

81. Turkbey B, Agarwal HK, Shih J, Bernardo M, McKinney YL, Daar D, et al. A Phase I Dosing Study of Ferumoxytol for MR Lymphography at 3 T in Patients With Prostate Cancer. AJR American journal of roentgenology. 2015; 205(1):64–9. [PubMed: 26102381]

82. Sankineni S, Smedley J, Bernardo M, Brown AM, Johnson L, Muller B, et al. Ferumoxytol as an intraprostatic MR contrast agent for lymph node mapping of the prostate: a feasibility study in non-human primates. Acta radiologica (Stockholm, Sweden : 1987). 2015

83. Hasan D, Chalouhi N, Jabbour P, Dumont AS, Kung DK, Magnotta VA, et al. Early change in ferumoxytol-enhanced magnetic resonance imaging signal suggests unstable human cerebral aneurysm: a pilot study. Stroke. 2012; 43(12):3258–65. [PubMed: 23138441]

84. Wagner S, Schnorr J, Ludwig A, Stangl V, Ebert M, Hamm B, et al. Contrast-enhanced MR imaging of atherosclerosis using citrate-coated superparamagnetic iron oxide nanoparticles: calcifying microvesicles as imaging target for plaque characterization. Int J Nanomedicine. 2013; 8:767–79. [PubMed: 23450179]

85. Budjan J, Neudecker S, Schock-Kusch D, Kraenzlin B, Schoenberg SO, Michaely HJ, et al. Can Ferumoxytol be Used as a Contrast Agent to Differentiate Between Acute and Chronic Inflammatory Kidney Disease?: Feasibility Study in a Rat Model. Investigative radiology. 2016; 51(2):100–5. [PubMed: 26352750]

86. Rogers JL, Tarrant T, Kim JS. Nanoparticle-based diagnostic imaging of inflammation in rheumatic disease. Current rheumatology reviews. 2014; 10(1):3–10. [PubMed: 25229498]

87. Simon GH, von Vopelius-Feldt J, Fu Y, Schlegel J, Pinotek G, Wendland MF, et al. Ultrasmall supraparamagnetic iron oxide-enhanced magnetic resonance imaging of antigen-induced arthritis: a comparative study between SHU 555 C, ferumoxtran-10, and ferumoxytol. Invest Radiol. 2006; 41(1):45–51. [PubMed: 16355039]

88. Neuwelt A. Ferumoxtyol Negatively Enhances T2-weighted MRI od Pedal Osteomyelitis in vivo. Journal of magnetic resonance imaging : JMRI. 2016

89. Neuwelt A, Sidhu N, Hu CA, Mlady G, Eberhardt SC, Sillerud LO. Iron-based superparamagnetic nanoparticle contrast agents for MRI of infection and inflammation. AJR American journal of roentgenology. 2015; 204(3):W302–13. [PubMed: 25714316]

90. Moy MP, Sauk J, Gee MS. The Role of MR Enterography in Assessing Crohn's Disease Activity and Treatment Response. Gastroenterology research and practice. 2016; 2016:8168695. [PubMed: 26819611]

91. Luhar A, Khan S, Finn JP, Ghahremani S, Griggs R, Zaritsky J, et al. Contrast-enhanced magnetic resonance venography in pediatric patients with chronic kidney disease: initial experience with ferumoxytol. Pediatric radiology. 2016

92. Uslu L, Donig J, Link M, Rosenberg J, Quon A, Daldrup-Link HE. Value of 18F-FDG PET and PET/CT for evaluation of pediatric malignancies. Journal of nuclear medicine : official publication, Society of Nuclear Medicine. 2015; 56(2):274–86.

93. Marso SP, Hiatt WR. Peripheral arterial disease in patients with diabetes. Journal of the American College of Cardiology. 2006; 47(5):921–9. [PubMed: 16516072]

94. Nathan DP, Tang GL. The impact of chronic renal insufficiency on vascular surgery patient outcomes. Seminars in vascular surgery. 2014; 27(3–4):162–9. [PubMed: 26073826]

95. Bashir MR, Jaffe TA, Brennan TV, Patel UD, Ellis MJ. Renal transplant imaging using magnetic resonance angiography with a nonnephrotoxic contrast agent. Transplantation. 2013; 96(1):91–6. [PubMed: 23680931]

96. Sigovan M, Gasper W, Alley HF, Owens CD, Saloner D. USPIO-enhanced MR angiography of arteriovenous fistulas in patients with renal failure. Radiology. 2012; 265(2):584–90. [PubMed: 22875796]

97. Alam SR, Shah AS, Richards J, Lang NN, Barnes G, Joshi N, et al. Ultrasmall superparamagnetic particles of iron oxide in patients with acute myocardial infarction: early clinical experience. Circ Cardiovasc Imaging. 2012; 5(5):559–65. [PubMed: 22875883]

98. Yilmaz A, Dengler MA, van der Kuip H, Yildiz H, Rosch S, Klumpp S, et al. Imaging of myocardial infarction using ultrasmall superparamagnetic iron oxide nanoparticles: a human study using a multi-parametric cardiovascular magnetic resonance imaging approach. European heart journal. 2013; 34(6):462–75. [PubMed: 23103659]

99. Han F, Rapacchi S, Khan S, Ayad I, Salusky I, Gabriel S, et al. Four-dimensional, multiphase, steady-state imaging with contrast enhancement (MUSIC) in the heart: a feasibility study in children. Magnetic resonance in medicine. 2015; 74(4):1042–9. [PubMed: 25302932]

100. Cheng JY, Hanneman K, Zhang T, Alley MT, Lai P, Tamir JI, et al. Comprehensive motion-compensated highly accelerated 4D flow MRI with ferumoxytol enhancement for pediatric congenital heart disease. Journal of magnetic resonance imaging : JMRI. 2016; 43(6):1355–68. [PubMed: 26646061]

101. Hanneman K, Kino A, Cheng JY, Alley MT, Vasanawala SS. Assessment of the precision and reproducibility of ventricular volume, function, and mass measurements with ferumoxytol-enhanced 4D flow MRI. Journal of magnetic resonance imaging : JMRI. 2016

102. DeSart K, O'Malley K, Schmit B, Lopez MC, Moldawer L, Baker H, et al. Systemic inflammation as a predictor of clinical outcomes after lower extremity angioplasty/stenting. J Vasc Surg. 2015; 5(15):00954–4.

103. Okura H, Takagi T, Yoshida K. Therapies targeting inflammation after stent implantation. Curr Vasc Pharmacol. 2013; 11(4):399–406. [PubMed: 23905635]

104. Habets J, Zandvoort HJ, Reitsma JB, Bartels LW, Moll FL, Leiner T, et al. Magnetic resonance imaging is more sensitive than computed tomography angiography for the detection of endoleaks after endovascular abdominal aortic aneurysm repair: a systematic review. European journal of vascular and endovascular surgery : the official journal of the European Society for Vascular Surgery. 2013; 45(4):340–50.

105. Ersoy H, Jacobs P, Kent CK, Prince MR. Blood pool MR angiography of aortic stent-graft endoleak. AJR American journal of roentgenology. 2004; 182(5):1181–6. [PubMed: 15100115]

106. Ichihashi S, Marugami N, Tanaka T, Iwakoshi S, Kurumatani N, Kitano S, et al. Preliminary experience with superparamagnetic iron oxide-enhanced dynamic magnetic resonance imaging and comparison with contrast-enhanced computed tomography in endoleak detection after endovascular aneurysm repair. J Vasc Surg. 2013; 58(1):66–72. [PubMed: 23561434]

107. Corot C, Robert P, Idee JM, Port M. Recent advances in iron oxide nanocrystal technology for medical imaging. Advanced drug delivery reviews. 2006; 58(14):1471–504. [PubMed: 17116343]

108. Blockley NP, Jiang L, Gardener AG, Ludman CN, Francis ST, Gowland PA. Field strength dependence of R1 and R2* relaxivities of human whole blood to ProHance, Vasovist, and deoxyhemoglobin. Magnetic resonance in medicine. 2008; 60(6):1313–20. [PubMed: 19030165]

109. Landry R, Jacobs PM, Davis R, Shenouda M, Bolton WK. Pharmacokinetic study of ferumoxytol: a new iron replacement therapy in normal subjects and hemodialysis patients. American journal of nephrology. 2005; 25(4):400–10. [PubMed: 16088081]

110. Neuwelt EA, Varallyay CG, Manninger S, Solymosi D, Haluska M, Hunt MA, et al. The potential of ferumoxytol nanoparticle magnetic resonance imaging, perfusion, and angiography in central nervous system malignancy: a pilot study. Neurosurgery. 2007; 60(4):601–11. discussion 11–2. [PubMed: 17415196]

111. Akeson P, Nordstrom CH, Holtas S. Time-dependency in brain lesion enhancement with gadodiamide injection. Acta radiologica (Stockholm, Sweden : 1987). 1997; 38(1):19–24.

112. Aghighi M, Pisani LJ, Sun Z, Klenk C, Madnawat H, Fineman SL, et al. Speeding up PET/MR for cancer staging of children and young adults. European radiology. 2016
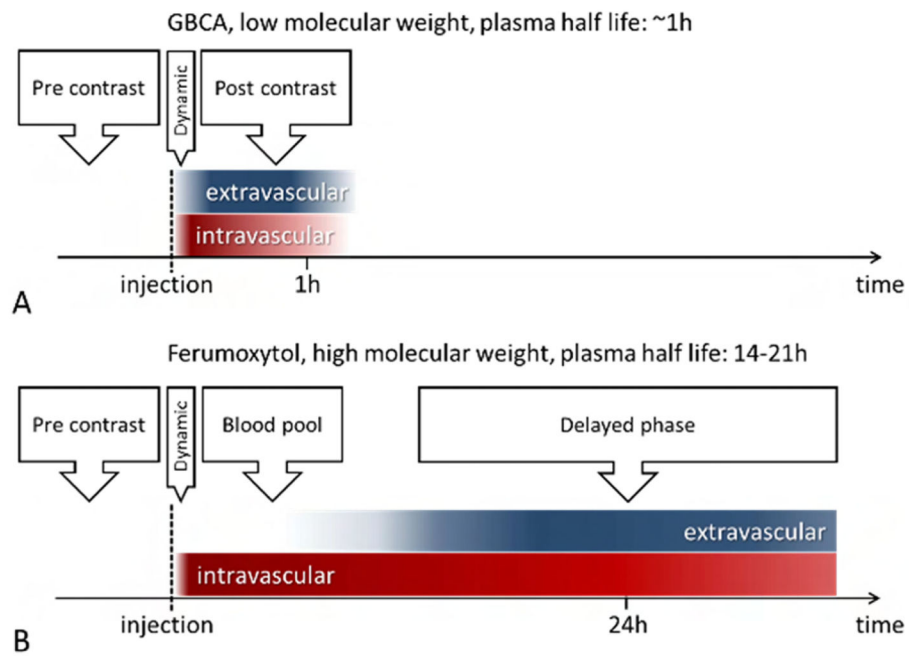
Figure 1.
Phases of GBCA (A) and ferumoxytol (B) enhancement. Unlike GBCA, ferumoxytol has a long intravascular half-life that results in a long blood pool phase prior to detectable contrast extravasation. GBCA (gadolinium based contrast agents). Images provided courtesy of Dr. Neuwelt.
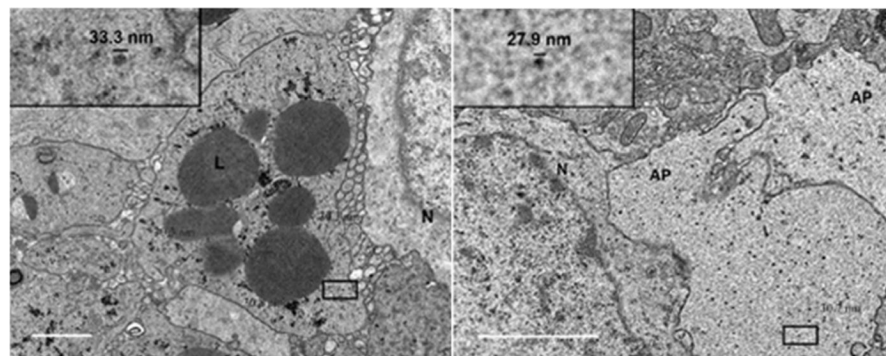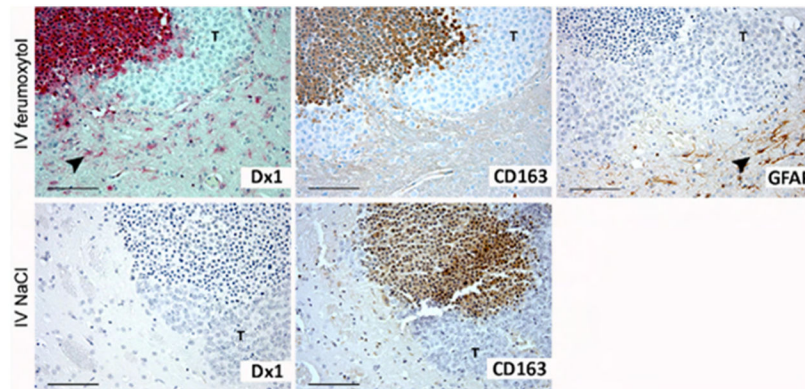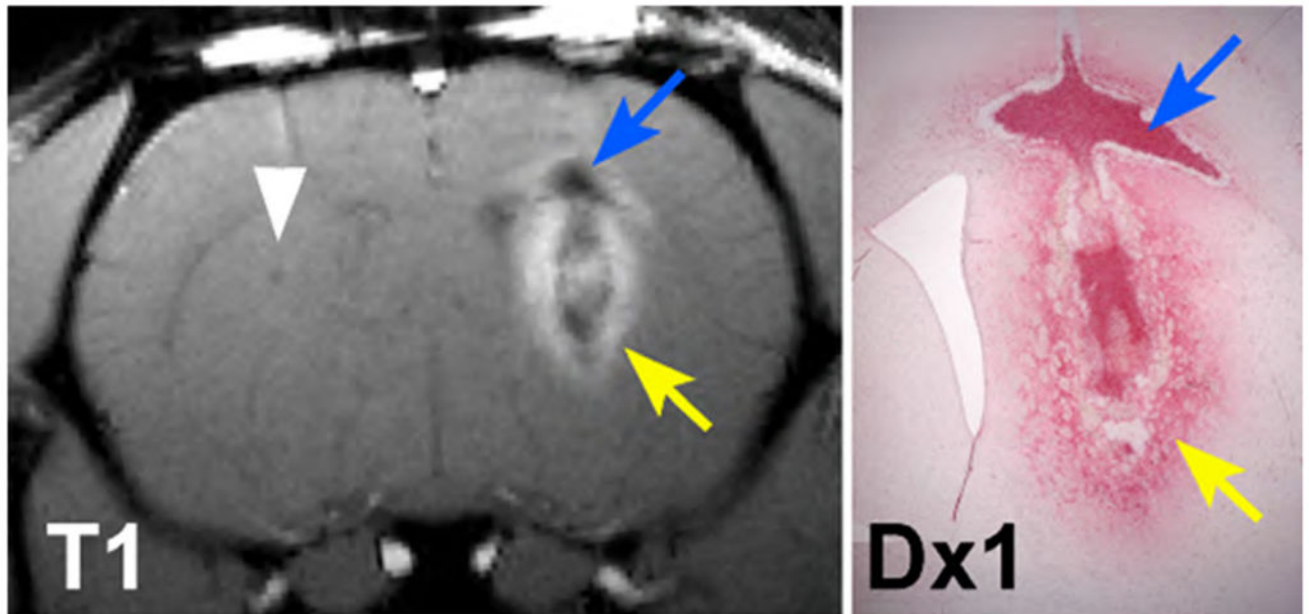
Figure 2.
Ferumoxytol traffics from systemic circulation to reactive lesions: immunocompetent rat xenograft model demonstrate sex travascular accumulation of ferumoxytol that correlated to the presence of activated macrophages.

A) MRI signal enhancement occurred in xenografted but not saline-injected hemispheres. Blue arrows show marked hypointense signal on T1 MR that correlates with histologic findings of intense immunostaining for ferumoxytol in macrophages using dextran-1. Yellow arrows show typical hyperintense enhancement on T1 MRI that correlates with diffuse milder staining for ferumoxytol in brain parenchyma and activated astrocytes using dextran-1. White arrowhead shows no signal change after saline injection in contralateral control hemisphere.

B) Immunostaining demonstrates that ferumoxytol traffics from the systemic circulation to reactive CNS lesions. Immunostains performed 48 h after H460 non-small cell lung carcinoma inoculation into caudate nucleus and 24 h after IV ferumoxytol administration. A representative inflammatory lesion was immunostained with dextran-1 (Dx1) for the ferumoxytol coating (red), CD163 for macrophages (brown), and GFAP for astrocytes (brown). All cell nuclei were counterstained with hematoxylin. T depicts live tumor cells. Arrowhead depicts reactive cells located outside of the main lesion. Scale bars, 100 μm.

C) Electron microscopy of a ferumoxytol laden macrophage (left) and two astrocyte processes (right). Left image: Iron oxide nanoparticles appear as electron-dense particles measuring ~30 nm in diameter located cytoplasmically and clustering around lysosomes (L). Right image: Two astrocyte processes (AP) showing dispersed, electron-dense ferumoxytol nanoparticles. N depicts neurons. Insets in both photos show a 27–33 nm diameter particle. Magnification 6800X, scale bar, 1 μm.

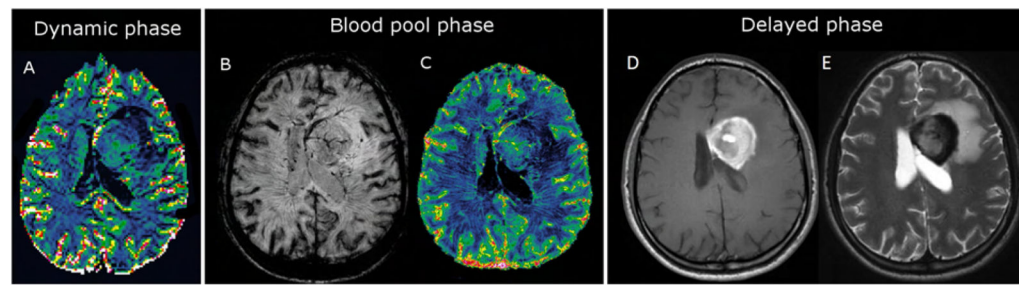From McConnell et al, 2016 used with permission from Nanomedicine: Nanotechnology, Biology and Medicine.

Figure 3.
Possible sequences with ferumoxytol in the CNS during the dynamic (A), blood pool (B, C), and delayed (D, E) phases after administration in a patient with newly diagnosed PCNSL. A: CBV map calculated from DSC perfusion with ferumoxytol shows mildly elevated rCBV within the neoplasm. B: Susceptibility weighted image shows curvilinear branching hypointensities compatible withs abnormal tumor vasculature. C: SS-CBV map with high resolution shows increased blood volume. D: Axial T1 MR demonstrates typical enhancement 24 hours after ferumoxytol injection. E: Axial T2 MR shows marked hypointensity within the tumor 24 hours after ferumoxytol administration. Images provided courtesy of Dr. Neuwelt.
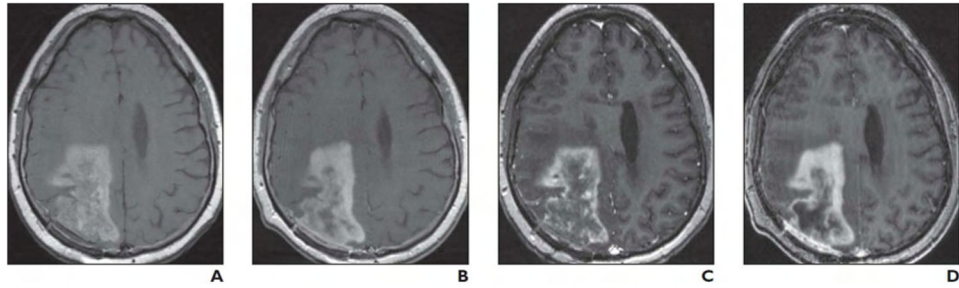
Figure 4.
Axial brain MRI of 19-year-old man who had undergone previous radiation and chemotherapy for glioblastoma multiforme, with clinical suspicion for pseudoprogression. A: Spin-echo (SE) T1 MR obtained 24 h after ferumoxytol administration shows moderately intense enhancement. B: SE T1 gadoteridol-enhanced MR shows concordant enhancement size and intensity. C: Magnetization-prepared rapid gradient-echo (MPRAGE) MR performed 24 h after ferumoxytol administration shows moderate (though less homogeneous) enhancement intensity compared with SE image. D: Gadoteridol-enhanced MPRAGE shows more homogeneous and greater enhancement intensity than the ferumoxytol-enhanced MPRAGE scan. Administered ferumoxytol dose was 510 mg (Hamilton et. al. 2011). From Hamilton et al. 2011, used with permission from AJR.
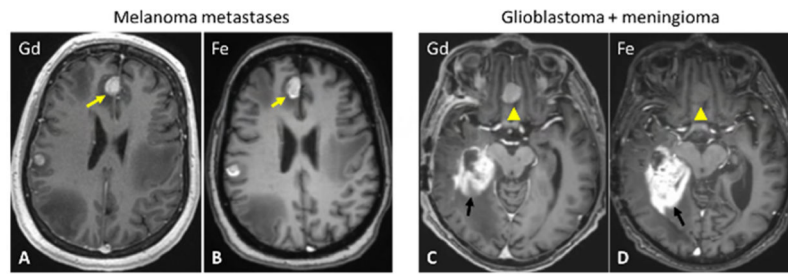
Figure 5.
Axial T1-weighted post contrast MRI images in two different patients with similar appearing frontal midline lesions. The mass (yellow arrows) enhances similarly with both Gd and Fe in a patient with melanoma metastases (A, B). A meningioma (yellow arrowheads) only enhances with Gd (C), not Fe (D) Of note, the glioblastoma in the same images (black arrows) enhances avidly with both agents (C, D). Images provided courtesy of Dr. Neuwelt.
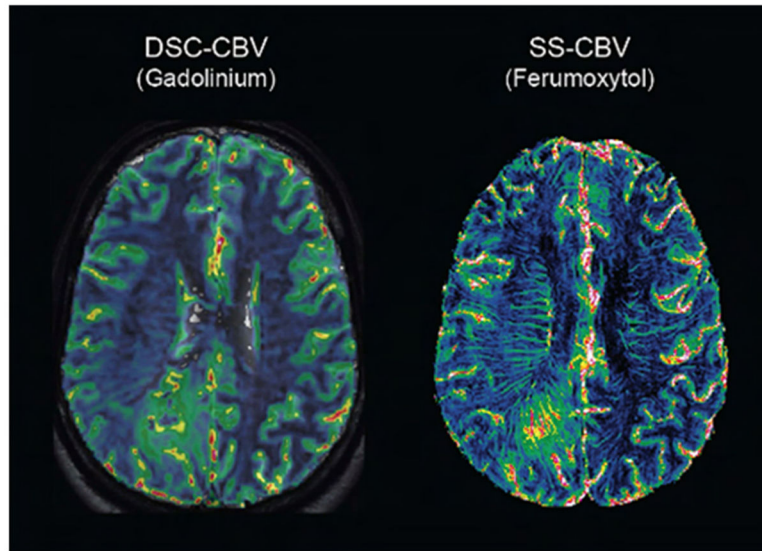
Figure 6.
SS-CBV maps using ferumoxytol offer higher spatial resolution and allow better identification of hypervascular areas for surgical targeting in glioblastoma patients. Compare spatial resolution of cerebral blood volume (CBV) maps using DSC PWI with a standard dose of gadolinium (DSC-CBV) (left) and SS ferumoxytol CBV map using ferumoxytol (3 mg/kg). The scan on the right more clearly demonstrates a central hypervascular area in the right occipital hemisphere with the greatest vascularity, which is likely the most malignant portion of the tumor. Images provided courtesy of Dr. Neuwelt.
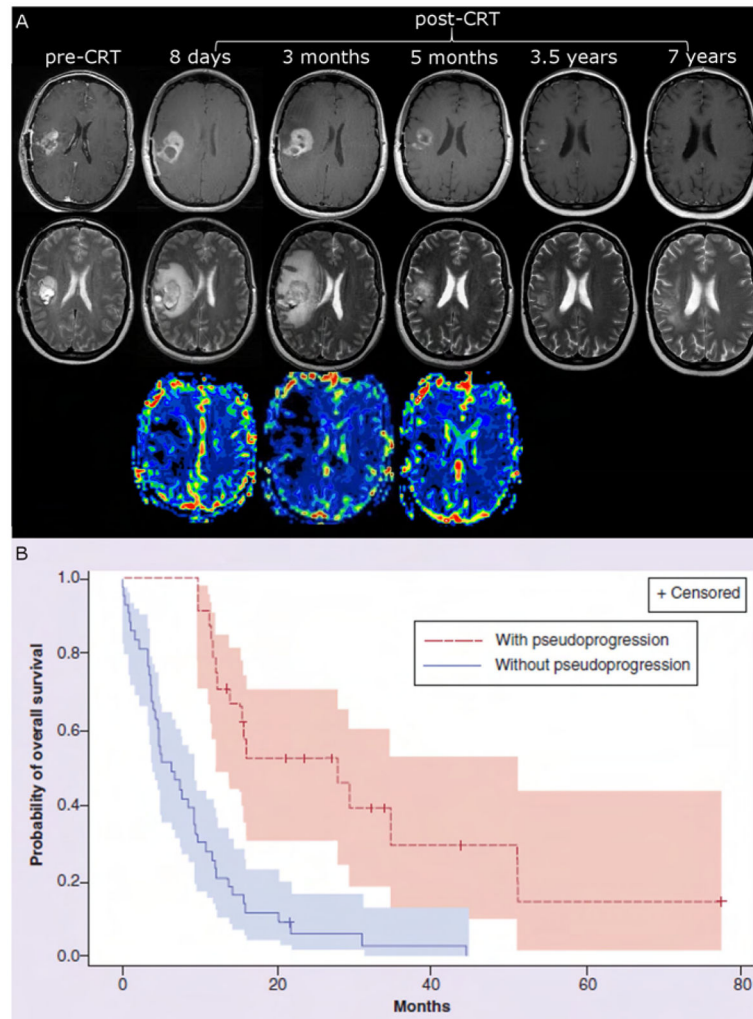
Figure 7.
Pseudoprogression can be diagnosed using perfusion MRI with ferumoxytol and correlates with OS.

A) Axial MR images of a 47-year-old woman with glioblastoma. Patient underwent T1-weighted sequences post Gd and T2-weighted postoperative images prior to CRT. Eight days after CRT completion patient scans showed radiographic worsening followed by further deterioration on follow-up MRI while the patient continued to receive adjuvant temozolomide chemotherapy. Though updated Response Assessment in Neuro-Oncology Working Group (RANO) criteria would indicate true tumor progression, the blood volume of the lesion was low on ferumoxytol DSC-CBV maps, which instead indicates pseudoprogression. The patient received only 3 courses of bevacizumab and continued adjuvant temozolomide. Substantial improvement is seen on 5-month follow-up MRI after completion of bevacizumab therapy. Seven years after completion of CRT, the image indicates that the patient is stable without evidence of recurrence/progression (the patient is still on adjuvant temozolomide chemotherapy).

B) Kaplan-Meier estimates of overall survival by the presence or absence of pseudoprogression. CRT: Chemoradiotherapy.
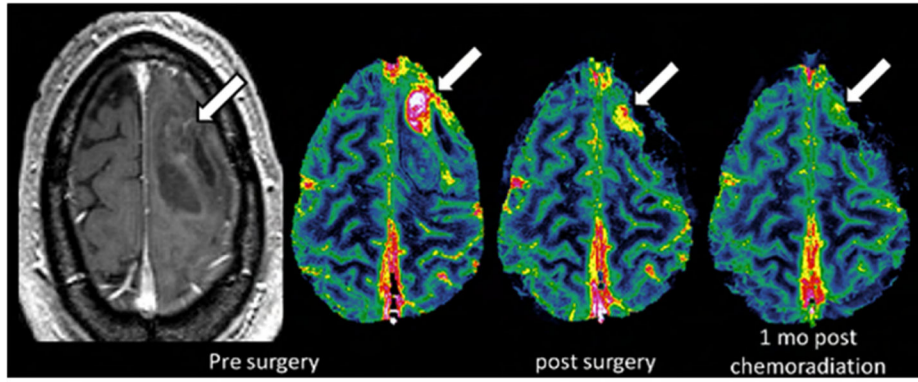From Gharamanov et al. 2014, modified with permission from CNS Oncology.

Figure 8.
42 year old male patient with glioblastoma. T1-weighted post gadoteridol scan shows no/minimal enhancement. In contrast, a highly vascular area (arrow) is seen on the high resolution steady-state CBV maps obtained with ferumoxytol. Residual tumor with high CBV shows reduction post chemoradiation therapy (post-surgery scan), and continued decrease on 1 month post chemoradiation scan, indicating treatment response. Images provided courtesy of Dr. Neuwelt.
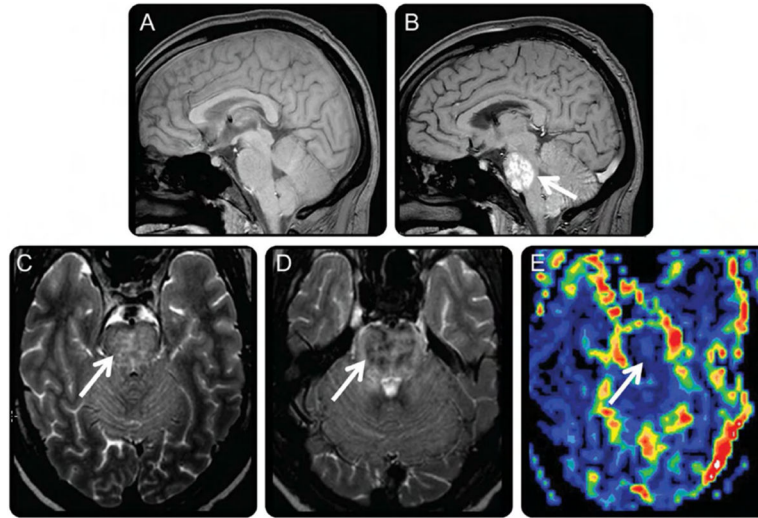
Figure 9.

A) Patient with the suspicion of pontine glioma was diagnosed with pontine demyelination using ferumoxytol. Precontrast T1-weighted imaging shows little abnormality.

B) T1-weighted sagittal MRI 24-hours post-USPIO shows diffuse intense enhancement due to ferumoxytol uptake in the pons (arrow).

C) Axial noncontrast T2-weighted MR shows patchy nonspecific increased T2 signal within the pons (arrow).

D) Axial T2-weighted MR obtained 24 hours post-ferumoxytol shows patchy hypointensities in the pons (arrow) correlating with ferumoxytol uptake.

E) Ferumoxytol-based DSC perfusion imaging shows low rCBV centrally within the pons (arrow) corresponding to the area of enhancing abnormality that is similar to normal-appearing white matter, a finding supportive of demyelination rather than high grade primary CNS neoplasm. DSC = dynamic susceptibility-weighted contrast-enhanced; GBCA = gadolinium-based contrast agent; rCBV = relative cerebral blood volume; USPIO = ultrasmall superparamagnetic iron oxide.

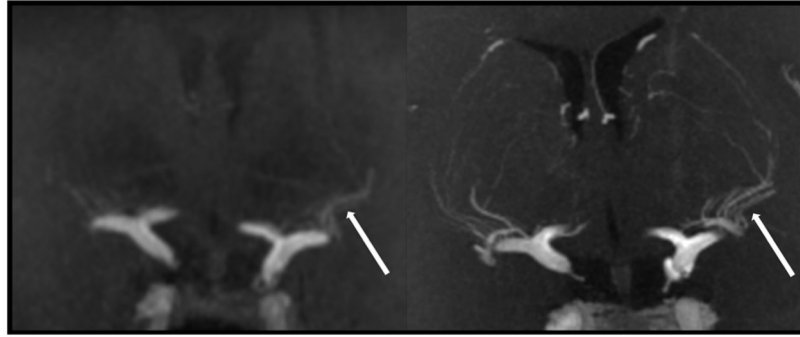From Farrell et al. 2013, used with permission from Neurology.

Figure 10.
Ferumoxytol MR angiography improves visualization of cerebral microvasculature when compared to Gadolinium at 7T field strength. Gadolinium-enhanced 3D T1-weighted gradient echo volumetric interpolated brain examination (VIBE) MRA of the supraclinoid internal carotid arteries (left) shows faint visualization of lenticulostriate vessels (white arrows). Ferumoxytol-enhanced MRA (right) demonstrates markedly improved visualization of the lenticulostriate microvasculature (white arrows). Images provided courtesy of Dr. Barajas.
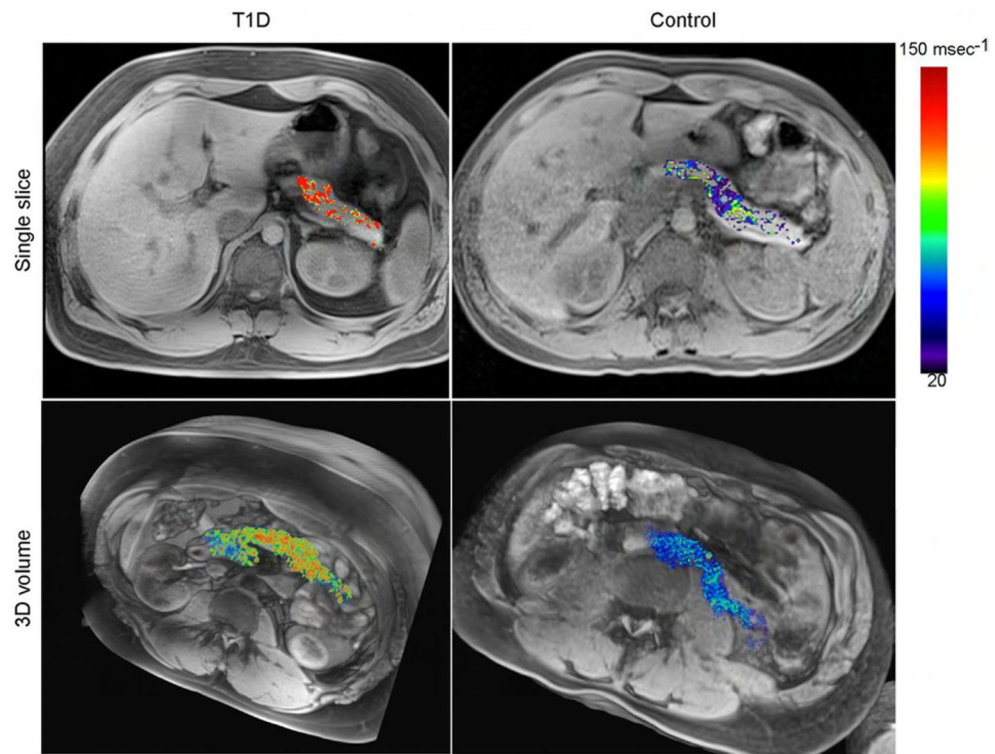
Figure 11.
Increased pancreatic nanoparticle accumulation in patients with type 1 diabetes (T1D). Single-slice (upper row) and 3D volume sets (lower row) of a representative patient with recently diagnosed T1D (left) and a normal control subject. From Gaglia et al., 2015 used with permission of PNAS.
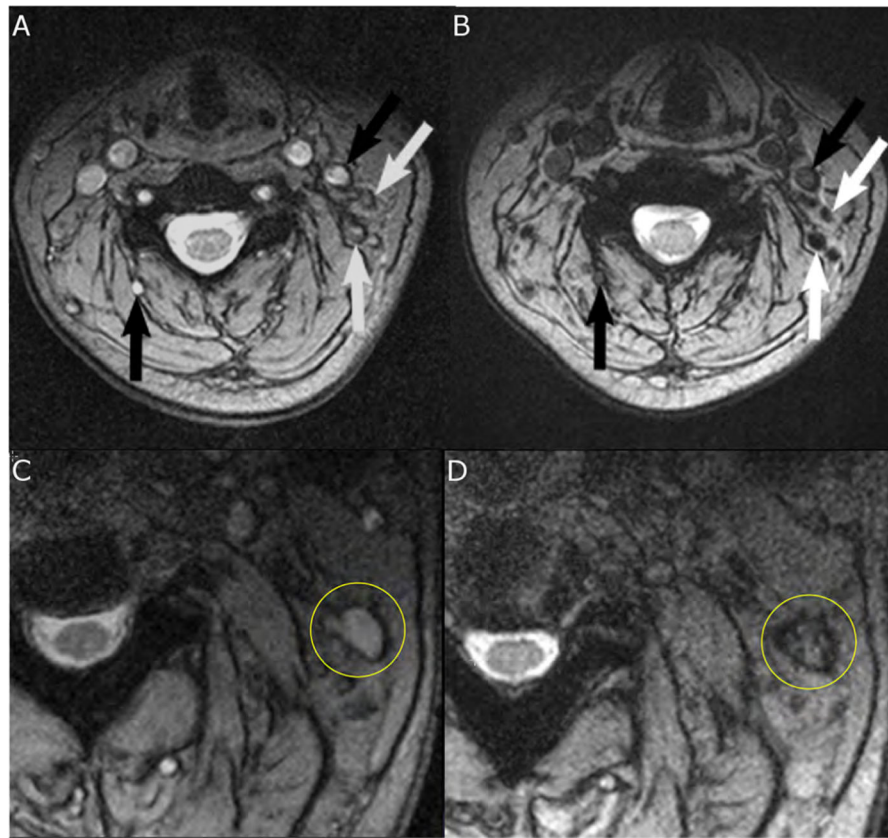
Figure 12.
Benign (A and B) and malignant (C and D) nodal patterns. Axial T2* GRE pre (A) shows intranodal high signal (white arrow) compared to hypointensity on 24 hours post (B) ferumoxytol scan, indicative of normal lymph nodes. Axial T2* GRE shows normal high precontrast intranodal signal (circle, C) compared to internal intranodal speckling (circle, D) suggesting a pathologic lymph node (black arrows indicate vascular structures). Images provided courtesy of Dr. Hamilton.

No.	Post Dose	Description	Diagnosis
#1		No blackening of node or node is hyperintense to surrounding tissue; heterogeneous or homogenous architecture	Metastatic
#2		Node has central high signal with darkening along the peripheral rim; heterogeneous architecture	Metastatic
#3		Partial darkening whereby more than 50% of the node has area of high signal intensity; heterogeneous architecture	Metastatic
#4		Less than 50% of node has high signal intensity; heterogeneous architecture	Possibly Metastatic
#5	fat fat	Node having an overall dark signal other than a central or hilar area of fat seen on T1 sequence; heterogeneous architecture	Non-metastatic
#6		Node having an overall dark signal with speckles of subtle granularities; homogenous architecture	Non-metastatic
#7		Node having an overall dark signal intensity; homogenous architecture	Non-metastatic

Figure 13.

Lymph nodes with an area of high signal intensity— encompassing the entire node or a large portion of it — are considered metastatic. A node with fatty hilum, complete signal void, and speckles of granularity without a definite focus of high signal intensity is considered non-metastatic. From Anzai et al., 2003 used with permission of Radiology.
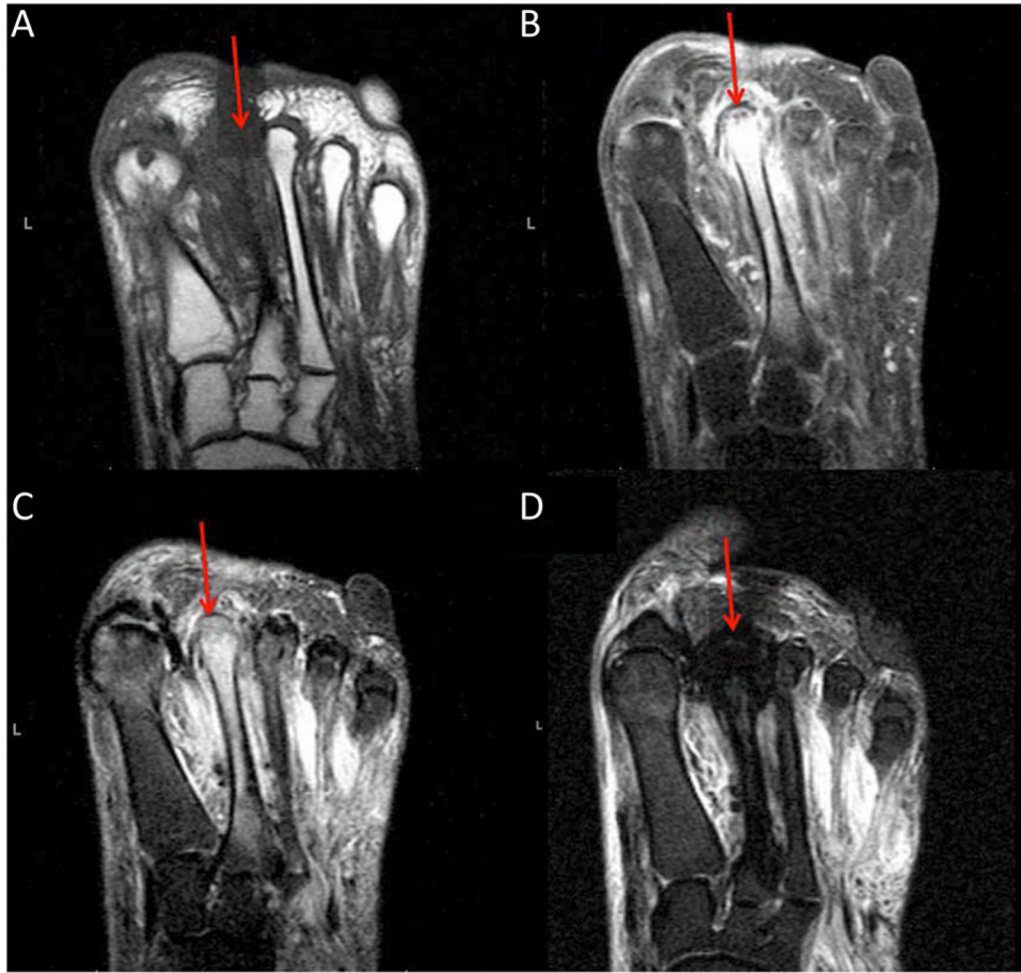
Figure 14.
Second metatarsal osteomyelitis in a 25-year-old patient with a history of a shotgun injury on the foot. T1-weighted noncontrast MR (A) shows hypointense signal involving the 2nd metatarsal (red arrow) and marked enhancement on gadolinium-enhanced T1-FS MR (B).. Noncontrast T2-weighted MR shows edema in the 2nd metatarsal (red arrow) and surrounding soft tissues (C. T2-weighted MR obtained 14 h after ferumoxytol administration (D) shows marked hypointensity compatible with ferumoxytol uptake, and consistent with the diagnosis of osteomyelitis. From A Neuwelt et al., 2016 used with permission of JMRI.

Figure 15.
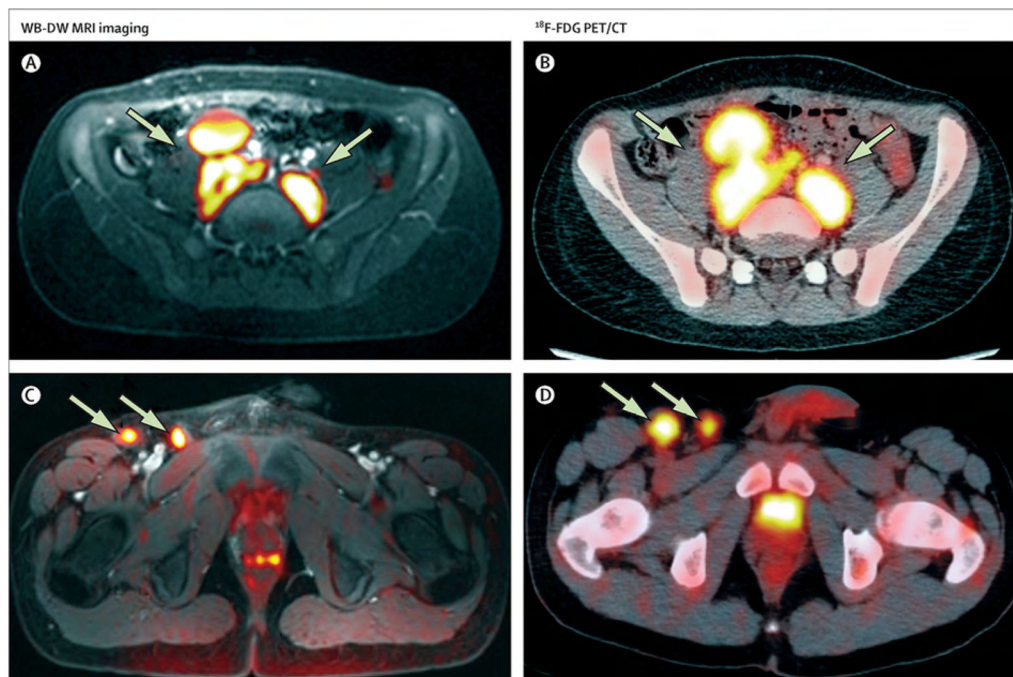Comparison of ionizing-radiation-free WB-DW MRI scans and 18F-FDG PET/CT scans for the detection of malignant lymphoma. (A) Axial WB-DW MRI and (B) 18F-FDG PET/CT scan of a 15-year-old patient with stage IIIA Hodgkin's lymphoma shows positive retroperitoneal lymph nodes (arrows). (C) Axial WB-DW MRI and (D) 18F-FDG PET/CT scan of a 14-year-old patient with class IIB Hodgkin's lymphoma shows positive right inguinal lymph nodes (arrows). Integrated ferumoxytol-enhanced WB-DW MR images provided equal sensitivities and specificities for cancer staging compared to 18F-FDG-PET/CT (28). More recent developments marry advantages of both imaging technologies towards 18F-FDG- PET/MR applications wherein ferumoxytol-enhanced anatomical T1-weighted MR images are merged with 18F-FDG-PET images (112). On 18F-FDG-PET/MR scans, ferumoxytol can help to differentiate malignant lymph nodes (18F-FDG positive, no iron uptake) from benign, inflammatory nodes (18F-FDG positive and iron uptake) as well as neoplastic bone marrow disease (18F-FDG positive, no iron uptake) from normal hypercellular hematopoietic marrow (18F-FDG positive and iron uptake) WB-DW=whole-body diffusion-weighted. 18F-FDG=18F-fluorodeoxyglucose. From Klenk et al., 2014 used with permission of The Lancet Oncology.

Figure 16.
Kawasaki Disease. Multi-lobed Aneurysms (arrows) of the Right and Left Coronary Arteries in a 3 year-old patient. Single frame from a MUSIC acquisition (99). Systemic arteries are colored red. Images provided courtesy of Dr. Finn.

Figure 17.
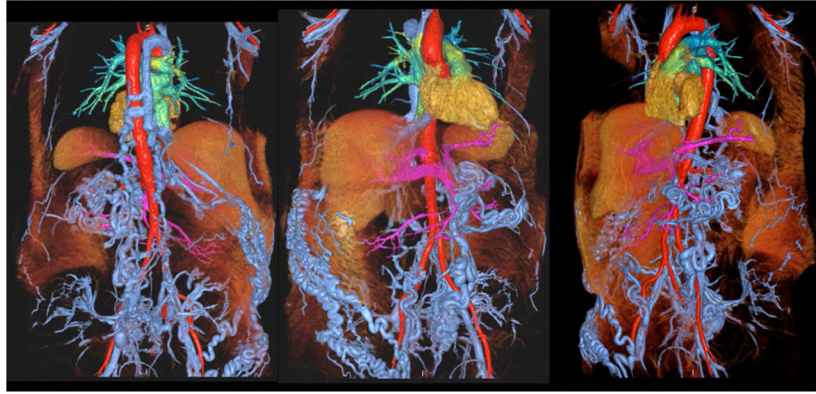Volume rendered reconstruction of an inferior vena cava occlusion in a 58-year-old male with chronic renal failure. Steady-state, breath held, high resolution MRA with ferumoxytol at 3.0 T. Huge pelvic and abdominal wall collaterals are clearly visualized, as well as a dilated azygous vein. Blue: systemic veins; Purple: portal vessels purple; Red: systemic arteries. Images provided courtesy of Dr. Finn.

Table 1

Comparison between ferumoxytol and gadolinium

Feature	Ferumoxytol	Gd-DTPA (Magnevist)
Basic element	Iron oxide	Gadolinium(III)
Molecular composition	Iron oxide coated with semisynthetic carbohydrate	Gadolinium chelated with diethylenetriamine pentaacetic acid
Relaxometric properties at 1.5 T. mM^{-1} s^{-1}, 37°C in water	r_1=15, r_2=89 (107)	r_1=3.3, r_2=3.9 (108)
Elimination plasma half-life	14 h (109)	1.6 h
Relative size of the particle	Around 30 nm (109)	0.357 nm
Permeability to intact BBB	Minimal	Minimal
Typical times to peak enhancement (in brain lesions)	24 h (110)	3.5–25 min (111)
Signal change on T1-weighted sequence	Increased signal (signal decrease at very high concentrations)	Increased signal
Signal change on T2-weighted sequence	Decreased signal	Usually no change
Signal change on T2*-weighted sequence	Decreased signal	Decreased signal if given as a bolus
Distribution	Dynamic phase, blood pool phase, delayed phase (extra and intracellular)	Dynamic phase, extracellular phase
Imaging dose	1–7 mg/kg	0.1 mmol/kg
Excretion	Stored with the body's iron reserve and used in hemopoesis. Coating with renal and faecal excretion.	Renal
Boxed warning	Potential hypersensitivity	Potential NSF

Table 2

Applications of ferumoxytol in CNS imaging

MRI sequences		Use	Advantages	Disadvantages
Dynamic phase	DSC perfusion	DDx based on lesion vascularity pre-operative grading prognosis assessment biopsy guidance therapy monitoring progression vs. pseudoprogression detection of recurrence/ malignant transformation stroke / hemodynamic assessment	low dose (1 mg/kg) needed no early contrast extravasation CBV, CBF, TTP, MTT, similar to CT/MR (gadolinium) perfusion	low spatial resolution susceptibility artifacts, distortions overestimation of large vessels (blooming) bolus administration needed
Blood pool phase	T2*-weighted (GRE)	improved visualization of abnormal vessels	improved visualization of small abnormal vessels no bolus injection needed no post processing needed part of most routine CNS protocols	susceptibility artifact motion sensitivity
	SS-CBV mapping (using pre- and post-Fe T2*w GRE scans)	DDx: ↑rCBV: HGG, PCNSL, metastasis ↓rCBV: LGG, demyelinaXon, toxoplasmosis, abscess pre-operative grading prognosis assessment biopsy guidance therapy monitoring detection of recurrence/ malignant transformation progression vs pseudoprogression	high spatial resolution thin slices, good 3D reformat for neuronavigation no distortions full brain coverage possible no bolus injection needed not influenced by circulation parameters repeatable potentially quantitative	susceptibility artifact motion sensitivity co-registration of the pre and post contrast images needed time consuming based on coverage (5–10 min)
Delayed phase	T1 enhancement (SE or MPRAGE) High SI	lesion visualization assessment of BBB damage DDx: meningioma vs metastasis intraoperative lesion assessment post-Sx residuum assessment without additional CA injection differentiating intra- and extracellular iron (39)	potential alternative to GBCA similar enhancement patterns as gadolinium in most pathologies prolonged enhancement (intra- and postoperative imaging without additional contrast agent administration)	additional scanning needed 24 h post ferumoxytol administration high concentration of ferumoxytol may result in T1 signal drop if enhancement persists it may mimic intracerebral blood
	T2 enhancement (T2w TSE) Low SI	assessment of BBB damage dg: meningioma vs metastasis intraoperative lesion assessment improved biopsy targeting differentiating intra- and extracellular iron	prolonged enhancement may indicate intracellular uptake of ferumoxytol	additional scanning needed 24 h post ferumoxytol administration if enhancement persists it may mimic intracerebral blood may be difficult to differentiate between intracellular iron vs. high concentration interstitial iron

DSC: dynamic susceptibility contrast. T2*w: T2*-weighted. GRE: gradient echo. SS-CBV mapping: steady-state cerebral blood volume mapping. Fe: ferumoxytol. GBCA: gadolinium-based contrast agents. SE: spin echo. MPRAGE: magnetization-prepared rapid gradient-echo. T2 TSE: T2 weighted turbo spin echo, DDx: differential diagnosis. Sx: surgery. BBB: blood brain barrier, CA: contrast agent, HGG: high grade glioma, LGG: low grade glioma, PCNSL: primary central nervous system lymphoma. CBV: cerebral blood volume. CBF: cerebral blood flow. TTP: time to peak. MTT: mean transit time. CNS: central nervous system. 3D: three-dimensional.

Table 3

Applications, advantages and the disadvantages of ferumoxytol enhanced MRI in patients with vascular diseases

Region	Possibilities	Advantages	Disadvantages
All modalities and general benefits and drawbacks	MRA and MRV Vessel wall visualization First-pass and steady-state images Whole body imaging	No ionizing radiation Nontoxic contrast agent Non-invasive Multiple planes Long imaging window (blood pool agent) Shows inflammation Highly reproducible	Close physiological monitoring necessary
Carotid and intracerebral arteries	Carotid CE-MRA - vascular integrity assessment - stenosis assessment - complete plaque morphology evaluation Circle of Willis (CoW) CE-MRA CoW evaluation for treatment planning Silent infarction demonstration	Direct visualization of the vessel wall Excellent soft-tissue contrast for plaque analysis More accurate in predicting degree of stenosis than DSA Plaque follow-up, progression monitoring	Close physiological monitoring necessary Not suitable for visualizing calcification
Aorta	Aneurysm Dissection Coarctation Endoleak Infective diseases diagnosis	Visualization of wall inflammation More sensitive for post EVAR endoleaks than CTA	Close physiological monitoring necessary
Cardiac	Coronary artery visualization Detection and remodeling of myocardial infarct Inflammatory diseases (myocarditis) Congenital heart diseases Chronic heart failure measurements Acute transplant rejection	High resolution and 3D images of the cardiac chambers and thoracic vessels Global and regional contractile function assessment Blood flow measurements High sensitivity and specificity for acute inflammation Response monitoring for treatment No breath holding Shorter acquisition time	Close physiological monitoring necessary Stents and metallic artifacts
Lower extremities	Lower limb CE-MRA Possibility for blood volume mapping Revascularization follow up	Post-revascularization increased blood volume can be shown	Difficulty in distinguishing arteries and veins on steady-state images
Visceral arteries	Renal artery evaluation Kidney transplant follow up Mesenteric ischemia Splenic artery aneurysm	Beneficial in any stage of renal insufficiency	
Veins	Vena cava and iliac vein thrombosis diagnosis and follow up Agenesis and chronic occlusion Vein mapping prior to dialysis graft placement	The whole abdominopelvic deep venous system is assessable Pulmonary thromboembolism can be visualized (in major vessels) Better sensitivity for thrombus imaging than non-contrast techniques No bolus needed Long imaging window Higher resolution Fewer motion artifacts High SNR	
Pediatric	Congenital heart disease Vascular malformations Kidney diseases and transplantation follow up	Whole body imaging is available	Sedation or anesthesia may be needed

MRA: magnetic resonance angiography. MRV: magnetic resonance venography. CE-MRA: contrast-enhanced MRA. CoW: Circle of Willis. DSA: digital subtraction angiography. EVAR: endovascular aneurysm repair. CTA: computed tomography angiography. SNR: signal to noise ratio.